FACULDADE DE ENGENHARIA DA UNIVERSIDADE DO PORTO

iHandU Simulator - Towards a medical education tool for wrist rigidity assessment

José João Serra de Brito Limpo Trigueiros

Mestrado Integrado em Engenharia Eletrotécnica e Computadores

Supervisor: Prof. Dr. João Paulo Cunha

Second Supervisor: Prof. Dr. Paulo Gomes Costa

February 24, 2020

Abstract

During Deep Brain Stimulation (DBS) surgery, electrodes are implanted in the patient's brain in order to alleviate symptoms of common motor disorders such as Essential Tremor (ET) and Parkinson's Disease (PD). Stimulation parameters and electrode position are adjusted during surgery, chosen in order to obtain the best improvement in the patient's symptoms. The most commonly assessed symptom is muscular rigidity, which is characterized by an increased resistance to movement marked by a permanently elevated muscle contraction in response to a passive stretch. The assessment typically results from a series of flexions and extensions of a chosen joint, and consists of a qualitative improvement given according to a subjective scale, which is susceptible to errors, and has a verified lack of consistency among different clinicians.

The solution to the quantization problem is under development in the form of decision support systems such as the iHandU, a wearable device in development at INESC-TEC. However, the assessment method used, as well as the clinician's personal experience both factor into the lack of inter-rater agreement in assessment results.

The remaining issue is in the lack of a standardized training method for clinicians outside of the clinical environment. This work focuses on the creation of a mechatronic simulator capable of mimicking passive wrist joint behavior in a patient undergoing DBS surgery, including wrist rigidity and cogwheel rigidity, enabling adjustment of these behaviors through system parameters and providing data comparable with the iHandU wearable device through use of similar sensors. Ultimately, this approach resulted in a rotary device capable of varying its joint mechanical impedance based on the sensed force, position data and defined system parameters.

Resumo

Durante a cirurgia de Estimulação Cerebral Profunda (ECP), são implantados eletrodos no cérebro do paciente de modo a aliviar sintomas de doenças neurológicas comuns, tais como o Tremor Essencial (TE) e a Doença de Parkinson (DP). Durante a cirurgia, a posição dos elétrodos e os parâmetros de estimulação são ajustados de modo a obter a maior melhoria nos sintomas do paciente. O sintoma mais frequentemente avaliado é a rigidez muscular, caracterizada por uma elevação permanente da contração muscular em resposta a um movimento passivo. Esta avaliação tipicamente provém de uma série de flexões e extensões efetuadas numa dada articulação, e consiste numa medida de melhoria qualitativa dada de acordo com uma escala subjetiva. Esta escala é susceptível a erros, e verifica-se inconsistência entre as avaliações de diferentes clínicos.

Uma solução para o problema de quantização encontra-se já em desenvolvimento através de dispositivos de apoio à decisão tais como o iHandU, um dispositivo vestível em desenvolvimento no INESC-TEC. Contudo, o método de avaliação utilizado, bem como a experiência pessoal do clínico, são fatores na falta de concordância entre clínicos nos resultados da avaliação. Deste modo, resta um problema na falta de um método consistente para o treino de clínicos, de forma estandardizada e fora do ambiente clínico.

Este trabalho visa a criação de um simulator mecatrónico capaz de imitar coportamentos passivos da articulação do pulso num paciente em cenário inter-operatório na cirurgia para ECP, como rigidez muscular e rigidez em roda-dentada, permitindo o ajuste destes comportamentos através de parâmetros de sistema, e a disponibilização de dados comparáveis com o dispositívo vestível iHandU através do uso de sensores semelhantes. Esta abordagem resultou num dispositivo rotatório com a capacidade de variar a impedância mecânica da sua articulação com base na força exercida, informação posicional e parâmetros de sistema definidos.

Acknowledgements

To Prof. Dr. João Paulo Cunha, I thank you for providing me with this opportunity, and for all your time and counsel provided as supervisor. Working with you, and the remainder of the INESC-TEC BRAIN team, has been an enriching experience at both an academic and personal level. In this note, Duarte, thank you for your guidance in these past few months, for showing me the ropes while allowing me to grow and acquire new skills.

To Prof. Dr. Paulo Costa, thank you for your insight regarding this work, and for the use of hobby electronics as a tool for education that truly changed my perception of the subject.

A great word of thanks to my friends. To the ones I've always had, and to the ones I'll keep forever. Sofia, thank you for your constant companionship along this journey far and wide. To André, Alex, Joca, Rui, Gintare, David, Inês, and fortunately so many others, for giving me the confidence and character I have today. To TEUP, and TUNAFE, for all of the incredible situations I'd have never dreamt of being in.

Among these friends, I am fortunate to count on my family. First, to my mother, who taught me that life cannot be strictly about achievements or failures, simple personal quantifications of our own fleeting joy and sorrow. In time, these will pass. Rather, it is about doing what we enjoy, treating every place and living thing with respect. The feelings we invoke in each other ripple among these places and living things, propagating through time. They will never be truly gone, as neither will you. And I owe much of my person to that.

To my father, who always pushed me to develop my skills. To my sister, who truly never forgot to visit, a most consistent company even from far away. To Mia and João, for always treating me as a son, and providing me with a home away from home. To all the others who played a part in this journey and who remain stuck with me for the next. My sincerest thanks.

José João Trigueiros

"Reminder that at your smallest components,
you are indistinguishable from a forest fire."

Night Vale Radio

Contents

List of Figures

Symbols and Abbreviations

ADC	Analog to Digital Converter
BRAIN	Biomedical Research And INnovation
C-BER	Center for Biomedical Engineering Research
CAD	Computer-Aided Design
DBS	Deep Brain Stimulation
DC	Direct Current
IC	Integrated Circuit
IDE	Integrated Development Environment
IPG	Implantable Pulse Generator
ISR	Interrupt Service Routine
I^2C	Inter-Integrated Circuit
MR Brake	Magnetorheological Brake
PCB	Printed Circuit Board
MRF	Magnetorheological Fluid
PD	Parkinson's Disease
PLA	Polylactic Acid
PWM	Pulse Width Modulation
UPDRS	Unified Parkinson's Disease Rating Scale

Chapter 1

Introduction

1.1 Motivation and Context

Parkinson's Disease (*PD*) and Essential Tremor (*ET*) are two very prominent neurobehavioral progressive movement disorders, as they have no known cure and tend to worsen with age. Symptoms for PD include tremors, muscular rigidity and bradykinesia (slowness of movement), whereas ET is characterized by involuntary tremors during the patient's voluntary movements, as well as muscular rigidity.

It is estimated that around 0.9% of the world population is diagnosed with ET – this figure increases to 4.6% for people over 60 years old [11]. Concerning PD, it is estimated that 0.1-0.2% of individuals worldwide are diagnosed with the condition. Its prevalence also increases with age, the figure increasing to 1% for people over 60 years old [21].

These diseases increasingly reduce the patient's quality of life as they progress, which affects not only the patient, but their close family and friends as well. Since there is no known cure, it becomes increasingly important to alleviate the symptoms of the disease as their severity grows.

Several efforts exist to alleviate their symptoms. Initially, the use of levodopa-based medication can be effective at alleviating the symptoms of PD, but as the disease progresses and higher doses are required, the periods during which the symptoms' attenuation is not overshadowed by the side-effects of the medication (referred to as "on" times) become increasingly shorter. [13]

Deep Brain Stimulation (*DBS*) is a therapy capable of alleviating some of these motor symptoms. It consists of an implantable pulse generator (*IPG*) installed typically under the skin of the upper chest, that sends electrical impulses through wire extensions threaded under the patient's skin and connected to thin wires tipped with electrodes (*leads*), which are implanted into deep brain targets. A representation of this setup is shown in figure 1.1. Electrical stimulation of these targets acts in a way that is currently not fully understood to alleviate some motor symptoms of PD, ET and similar conditions [13].

During the lead placement surgery, adjustments are made to the lead position, as well as the IPG parameters, such as voltage, pulse width and frequency. All of these factors affect the stimulation field, and are adjusted in order to search for the best patient response. Clinically, this

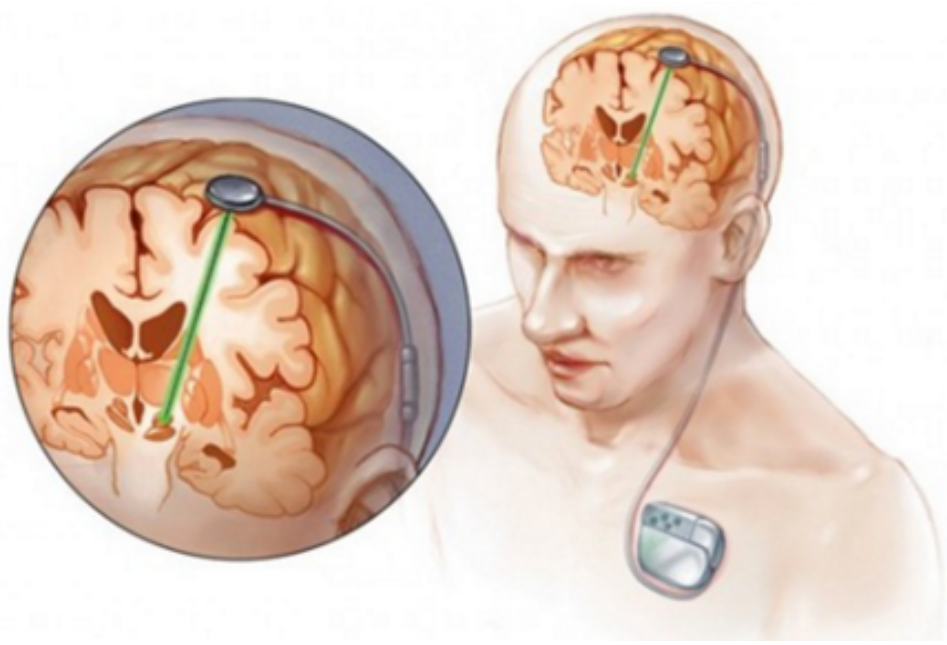

Figure 1.1: Deep Brain Stimulation setup. Source[1]

response is perceived through a muscular rigidity assessment. Rigidity can be defined as an increased resistance in response to a passive stretch, which is generated by antagonist muscles due to a permanently elevated muscle contraction.

This assessment is typically performed by a clinician, who induces a passive movement at the wrist or elbow of the patient, such as successive flexion and extension of the chosen joint. A score for improvement is then attributed, in accordance with a qualitative scale, such as the Unified Parkinson's Disease Rating Scale (*UPDRS*) [13]. This method is subjective, with evidence pointing to a lack of agreement among clinicians [5].

The problem of intra-operatory rigidity quantification is currently being addressed through use of decision support devices [3, 15, 17]. This work is written parallel to the development of a novel wearable medical device geared towards decision support at INESC-TEC by the name of iHandU [4, 10]. Further detailed in section 2.3, this portable, wearable device consists of a textile band equipped with an inertial sensor that rests in the patient's palm, as well as force sensors that rest in the back of the patient's hand. It is capable of quantifying improvements in muscular rigidity. This context provides several benefits, such as result comparison and the availability of clinical data.

In the context of this device's development, and during clinical trials for the device, a need has been verified for uniformity among the rigidity assessment methods of different clinicians, whose variations and experience (or lack thereof) factor into the verified lack of inter-rater agreement when it comes to assessment results. The development of such a uniform method can be facilitated by a medical education tool, such as a robotic simulator of the wrist joint of a patient undergoing

[1] https://www.extremetech.com/wp-content/uploads/2013/07/Deep-brain-stimulation-640x353.jpg

DBS surgery, with parameters to mimic different degrees of rigidity. Such a tool would provide the means to train clinicians consistently and uniformly in this matter.

My personal motivation for this work arises from my interest in the intersection of robotics and biomimetics, seen here in the replication of a physiological function through a robotic actuator. This work also strives toward the development of technology that may improve the efficacy of the rigidity assessment performed during DBS surgery, which in turn is a modern treatment (cf. figure 1.2) capable of improving the quality of life of patients suffering from prominent conditions such as PD or ET.

Figure 1.2: DBS in the cover of Público, a Portuguese daily national newspaper, ed. January 22nd, 2020[2]

1.2 Objectives

This work aims to create a device capable of simulating the passive wrist joint of a patient undergoing DBS surgery, with variable parameters that allow mimicking of the symptoms and their severity levels outside of the clinical environment.

In order to allow for data and model comparison between the robotic simulator and the iHandU device, the simulator must be equipped with sensors and algorithms similar to those present in the iHandU.

Considering the end goal of this simulator as a medical education tool, there is an implicit need for good replicability, and an encouragement for low material cost, so that copies of the device may be reproduced in both quantity and quality with little difficulty, provided access to all the source files.

On this note, the system is intended to simulate the passive joint of a patient undergoing an intra-operatory wrist rigidity assessment (cf. figure 2.2), and as such should provide a comfortable structure for the user, which will take the role of the real-case clinician, to perform such an assessment on the device.

1.3 Scientific Contributions

This work has resulted in the creation of a programmable, force-sensing wrist-like device capable of varying its mechanical impedance according to a set model, equipped with sensors akin to those of the iHandU for the testing of future rigidity identification algorithms in this context. The device is equipped with a fist-shaped segment analogous to the human hand in the rigidity assessment scenario, using similar proportions, and is intended for additional realism and user comfort.

The resulting simulator makes no pretense of providing a realistic mathematical model, but demonstrates the possibility for such an implementation through a comparison with the existing iHandU wearable signal and exposure to its classification algorithm. Some nonlinear characteristics found in the real case are also represented in the simulator's current implementation and are adjustable through a set of device parameters, such as cogwheel rigidity position, range, severity and directionality, and maximum joint flexion range.

1.4 Document Structure

Beyond the introductory chapter, this work is organized in three major parts, representing the preliminary research, prototype development and result analysis, as detailed below. A final chapter then presents some closing remarks, such as comments on the completion of the objectives mentioned in section 1.2, as well as some suggestions for future development.

[2] https://www.publico.pt/jornal?date=20200122

In chapter 2, the preliminary research on the state of the art is featured, providing an in-depth look at several concepts mentioned in section 1.1. Some existing similar or relevant work is shown as well, providing some guidance in designing a solution.

Then, in chapter 3, we explore some theoretical fundamentals related to components used in these similar works, alongside other fundamentals specific to our problem, such as wrist joint mechanics. We then take these concepts and visit the prototypes that resulted from their application, detailing their advantages and shortcomings, as well as our control strategy and sensor scale calibration methods.

Having obtained a suitable prototype, we move to discuss the results through the obtained output data in chapter 4. Having equipped our prototype with sensors similar to those of the iHandU, a comparison is performed between this simulator and the existing, clinically validated wearable devices.

Chapter 2

State of the Art

This chapter will provide an overview of the problem within the medical field, allowing for a proper understanding of our objectives and limitations in designing a solution. Furthermore, we will explore some relevant work in section 2.4, in order to understand how others have tackled similar problems in the past.

2.1 Deep Brain Stimulation

Deep Brain Stimulation (*DBS*) is a palliative treatment – its purpose is to lessen the motor symptoms of some currently incurable neurobehavioral and movement-related disorders. It was first approved by the Food and Drug Administration (*FDA*) as a treatment for the motor symptoms of PD and ET in 1997 [13], having since been approved for use in several other conditions, such as dystonia and epilepsy [19, 22].

The treatment consists of stimulating certain deep brain targets by using DBS leads, wires tipped with small electrodes. These leads are connected to an implantable pulse generator (*IPG*) through wire extensions, as the IPG is typically installed under the skin of the upper chest, as previously seen on figure 1.1.

The IPG sends electric signals to the selected electrodes, using variable parameters, such as voltage, pulse width and frequency, controlling the stimulation field that acts on these deep brain targets, as shown in figure 2.1. These adjustments to the stimulation field are made in order to better regularize brain activity in the affected circuits, promoting relief from several common symptoms such as muscular rigidity, tremor and bradykinesia, while minimizing any side effects from the stimulation. However, the exact way in which this procedure alleviates the symptoms of these conditions is not fully understood and, as such, it will generally take some time and several adjustments until the optimal set of parameters is found [13].

During the intra-operatory parameter adjustment process, the patient must be awake as their passive muscular response is monitored by a clinician, commonly by assessing the muscular rigidity on the patient's wrist joint [13].

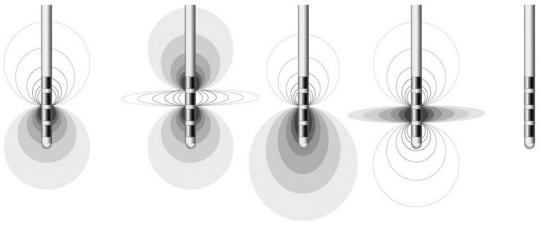

Figure 2.1: Example of different DBS electrode configurations. Adapted from [1]

2.2 Rigidity Assessment

Rigidity can be defined as a joint's increased mechanical impedance in response to a passive stretch. This occurs due to a permanently elevated muscular contraction in the region, which results in a higher difficulty of movement due to the contraction of antagonist muscles.

The rigidity assessment consists of the successive flexion and extension of the chosen joint, normally the wrist or elbow, by the clinician, who will attribute a score within a qualitative rigidity scale in accordance with their perception of the chosen joint's stiffness. During this evaluation, the patient is in a passive, awake state [13]. In other words, the patient should not attempt to assist or hinder the exercise performed by the clinician, so that the force felt by the clinician is an accurate representation of the mechanical impedance generated by the patient's involuntary muscular contractions. An example of such an exercise is depicted on figure 2.2.

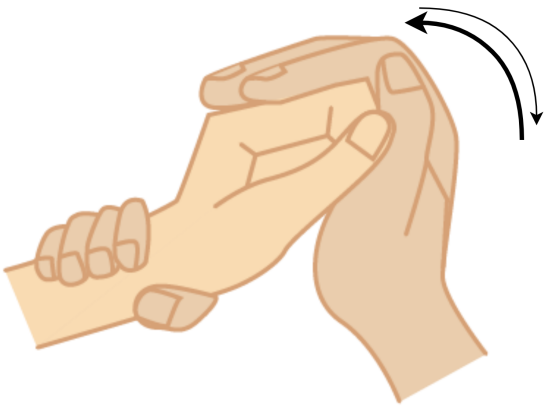

Figure 2.2: Example of a rigidity assessment exercise. Adapted from [2]

Cogwheel rigidity is a common artifact that aids the clinician in adequately classifying muscular rigidity. It may be defined as an accentuated heterogeneity in a given joint's response to a passive movement, or rather a limited area where the patient's muscular rigidity is noticeably higher, typically around the midpoint of the joint's flexion angle [6, 4, 10].

[1] https://i1.wp.com/www.neurosurgery-blog.com/wp-content/uploads/2012/11/Short-circuit-in-DBS.jpg?ssl=1
[2] https://www.saebo.com/wp-content/uploads/2017/03/4-Wrist-and-Hand-Flexion-and-Extension.png

The subjective assessment performed and imprecise scale used implies not only a loss in resolution, but also a detriment to its reliability. A review has shown that several studies point towards a lack of consistency among different clinicians' ratings [17]. These difficulties motivate the quantification of these symptoms' improvement, which is addressed by devices such as the iHandU, a wearable decision support device further detailed in section 2.3.

Variations in the assessment method and the clinician's personal experience, or lack thereof, are also held accountable for this lack of inter-rater consistency. This work focuses on the development of a robotic simulator to assist in the eventual creation and standardization of a consistent methodology for the uniform training of clinicians in wrist rigidity assessments. In this context, a review of notable mechanical simulators with similar properties to this objective is presented in section 2.4.

2.3 Assessment Support Systems

As a result of the subjective and oftentimes imprecise assessment methods used, several efforts exist in favor of quantifying rigidity objectively through a medical tool, either as evaluation methods or decision support systems [3, 15, 17]. Notably, one such decision support solution is under development at INESC-TEC, under the name iHandU. A portable, lightweight and relatively small wearable device, it is capable of reliably classifying muscular rigidity and detecting cogwheel rigidity through the analysis of signal characteristics [4, 10].

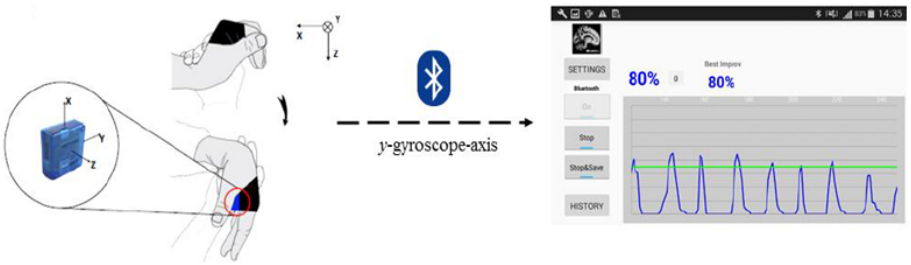

Figure 2.3: Example of a rigidity assessment assisted by the iHandU. Adapted from [10]

The iHandU provides a value for percentage of improvement by analysing kinematic data through an integrated circuit, featuring an accelerometer, gyroscope and magnetometer, and is capable of computing quaternions in real time. Signal data is transferred via Bluetooth to a compatible device. The assessment is performed through a signal descriptor that considers the gyroscope signal average and peaks. This descriptor is used as the input argument of a rigidity identification polynomial function developed for this purpose through collected clinical data. This results in the final assessment, which is presented in the form of a muscular rigidity improvement percentage, in the scale typically used by local clinicians. The device is also capable of detecting cogwheel artifacts in the movement by searching for suitably-sized oscillations and analysing their characteristics.

In collaborating with the development of the iHandU, this work gains access to much relevant data and resources, such as the device itself, its quantification algorithms and clinical data. This is very useful in the context of data comparison and discussion of results. Conversely, the robotic simulator resulting from this work may provide a way to simulate the wrist rigidity model at any time, outside of the clinical environment.

2.4 Existing Joint Simulators

The goal of this work is to simulate a patient's wrist joint in the aforementioned rigidity assessment scenario of intra-operatory DBS surgery. The patient is in an awake, yet passive state, as the clinician repeatedly flexes and extends the patient's wrist joint. We wish to create a device that is morphologically similar to the patient's arm, capable of simulating different levels of rigidity in the mechanical joint analogous to the elbow.

Other works related to robotic simulation of joints, or different motor conditions such as spasticity exist in the domain of physiotherapy [8, 12, 23], although no other attempts to create the type of simulator we intend have been verified at time of writing. These existing studies produced devices through use of principles and components of value to our application.

The types of simulators featured in the following subsections were designed to assist in the training of rehabilitation therapists by replicating motor symptoms of certain diseases. These types of devices are sometimes referred to as *part-task trainers* [23].

2.4.1 Haptic Simulator of Elbow Joint Spasticity

In the haptic elbow joint spasticity simulator by Grow et al. [8], a steady, robust metallic structure houses a motor and disc brake. A long, metallic, forearm-like structure is attached to the brake axle akin to a lever, and in its extremity is a plastic, child-like hand 2.4.

It is stated in the source material that the device is designed to replicate "the spastic elbow of a child" [8].

The brushed DC motor is connected to the brake caliper below it, in such a way that the brake control is performed by actuation of the motor. Position control is provided by an incremental encoder attached to the rotary joint. A spasticity model is then used to realistically control the system, and result validation is then performed based on the professional opinion of available practitioners.

This approach could be viable for our application, yet the wrist rigidity assessment typically requires a more complete grasp on the patient's hand in a point much closer to the device joint, as depicted on figure 2.2, which is an action that the disc brake would not appear to allow, in this configuration.

Furthermore, this simulator features a variety of custom parts and requires a considerable amount of assembly, such as the installation of the brake and motor, and the latter's connection

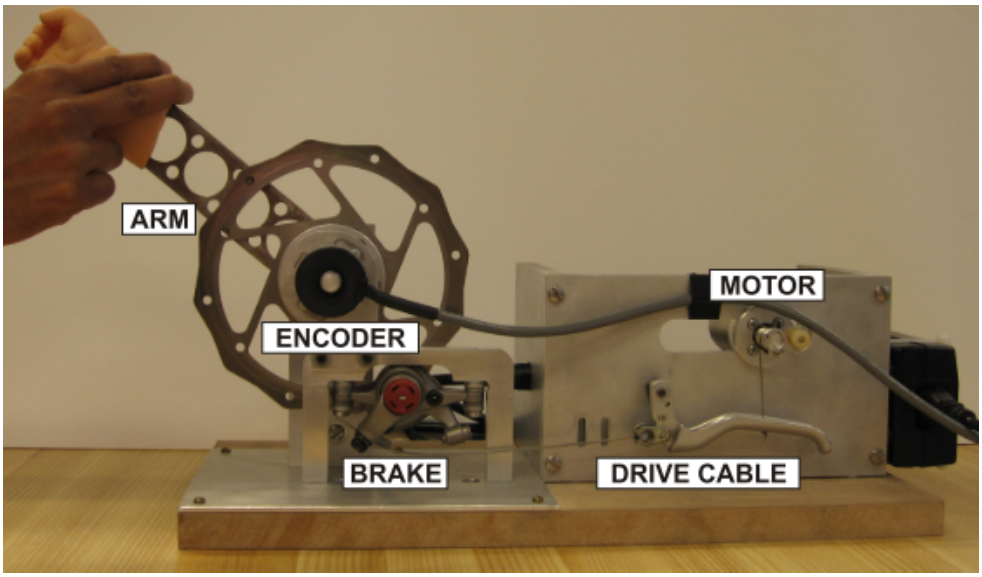

Figure 2.4: Elbow joint spasticity simulator by Grow et al. [8]

to the brake caliper. These are characteristics that impair our goal of *replicability*, as discussed in section 1.2.

In this work, the possibility of using a DC motor alone to emulate elbow resistance was excluded due to gearing, fidelity and size constraints [8]. However, our simulator aims to simulate the wrist joint, and as such, use of DC motors remains an option.

2.4.2 Upper Limb Disorder Emulator

The elbow emulator for therapy education by Zakaria et al. [23] is a complex, arm-like articulate structure actuated by an electric motor as well as a magnetorheological brake (*MR brake*). These components both actuate in the same axle, and the resulting force is transferred via a thick band through the interior of the skin-like silicone sleeve, to the mechanical joint analogous to the elbow. Additionally, a rotary encoder and strain gauge are employed for position control and force detection respectively.

The use of both a motor and brake allows for the simulation of an active patient, capable of moving their own arm while affected by the simulated condition.

Magnetorheologic (*MR*) brakes are a class of electrically activated brakes that apply magnetorheological fluid technology (*MRFT*) to apply a rotational mechanical impedance in the output shaft [2].

MR fluid may be defined as a non colloidal suspension of small, magnetizable, typically metallic particles in an inert base fluid. When exposed to a magnetic field, these metallic particles align themselves, altering the mechanical properties of the suspension – in the case of MR brakes, fluid is placed within the device in such a way that the mechanical impedance of the brake shaft varies in accordance with the intensity of the magnetic field produced through differing electrical inputs [2].

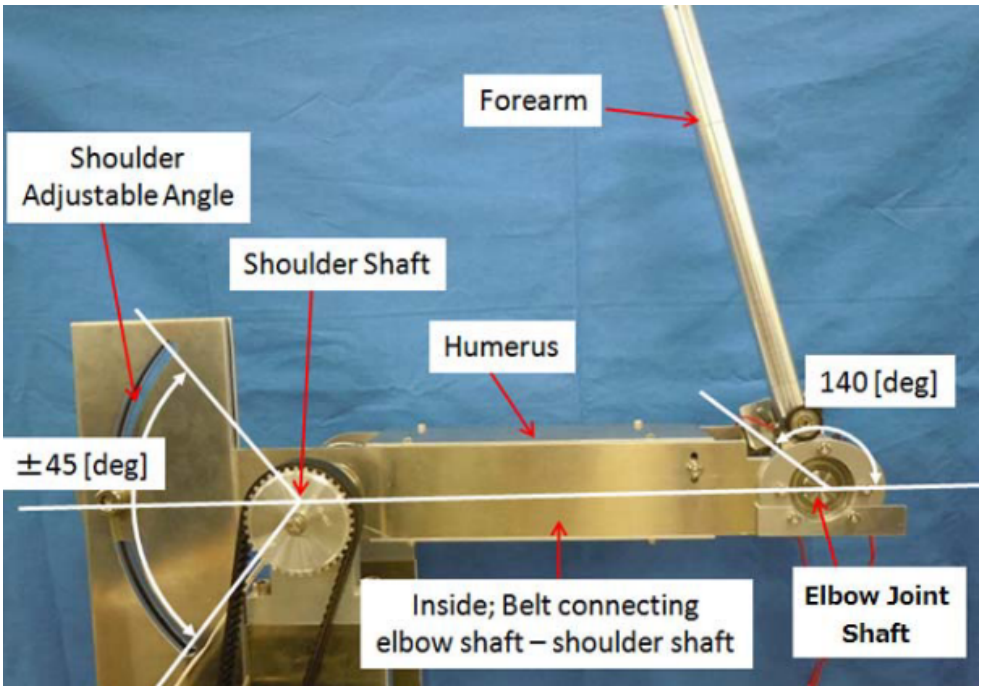

Figure 2.5: Elbow emulator for therapy education by Zakaria et al. - internal mechanism [23]

This type of brake is markedly more convenient for our application than the disc brake seen in the simulator by Grow et al. due to its compact structure and direct electrical actuation control, but is also significantly more expensive than using a simple DC motor, impairing our goal of producing a simulator with a reduced cost as discussed in section 1.2. Additionally, the MR fluid thickens with use and must be eventually changed, providing an additional complication in the form of a maintenance operation and eventual actuator uncertainty related to the variable fluid thickness.

Strain gauges like the one employed here are a useful, versatile technology for force sensing applications, providing an electrical signal that is sensibly proportional to the force applied to the strain gauge. Load cells are robust, force sensing devices built upon this principle and will be discussed in a future chapter.

The solution by Zakaria et al. makes use of some notable components that could be beneficial to our application, such as strain gauges, but its structure is quite complex, even more so than the simulator described in section 2.4.1, making use of an abundance of custom parts, including a pulley system and silicone sleeve, going against our need for an easily replicable system.

The use of MR brakes would possibly result in a better, albeit much more expensive simulator. Its advantages relative to the disc brake include ease of assembly, less moving parts, compact build and electrical actuation. In relation to a DC motor, it would be preferable as it is a passive actuator – a brake would be safer for the user in the event of an electrical malfunction. Despite this, the higher pricing of this technology weighs greatly upon our goal to create a low-cost simulator, as

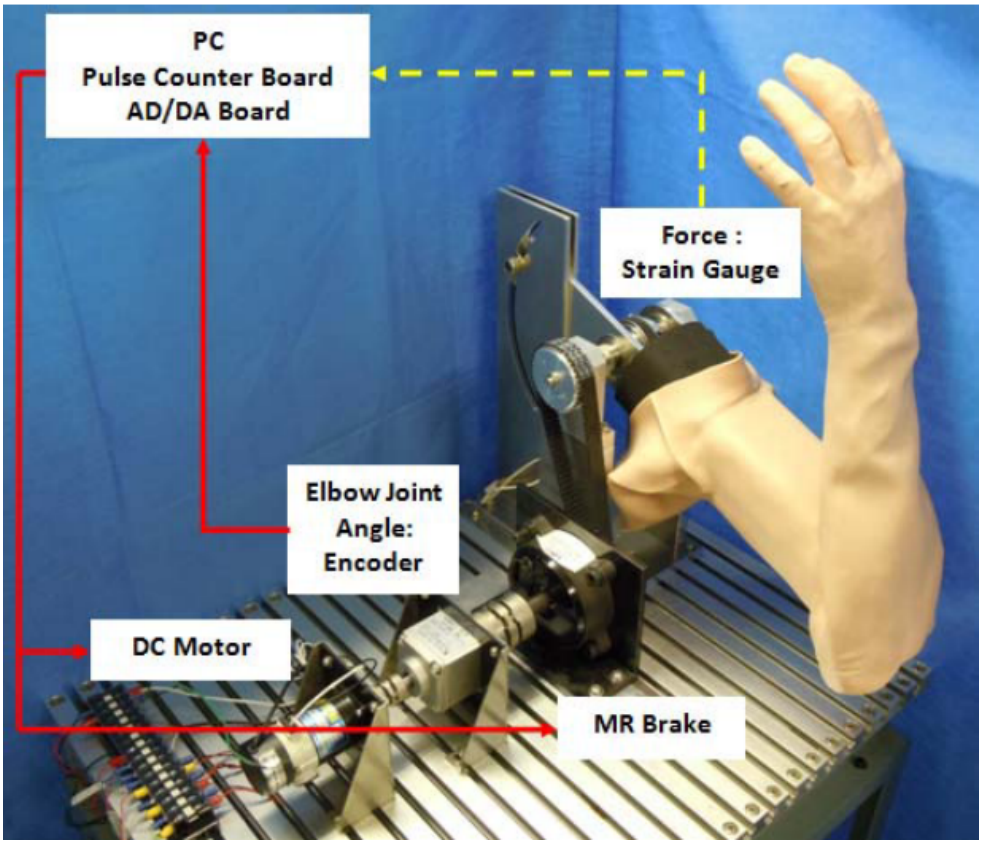

Figure 2.6: Elbow emulator for therapy education by Zakaria et al. - actuation and exterior [23]

described in section 1.2. The commercial solutions found to be considerably more costly than other actuation methods, and the MR fluid would have to be periodically changed in the long term, as it thickens with use [2]. However, it could be considered as an alternative if other solutions prove ineffective.

Finally, the use of both a brake and a motor is unnecessary for our passive application. By using a single, compact rotational actuator, the need for a pulley system could be avoided as the actuator could directly serve as the mechanical joint.

As a result of this analysis, we have not found a simulator that fits all the defined goals, although several useful concepts have been retained. In conclusion, this means that the present work will take on an exploratory nature by necessity, placing an emphasis on experimentation.

Chapter 3

System Design and Implementation

In this chapter, the prototype development is presented, beginning with relevant theoretical principles stemming from the preliminary research performed in chapter 2, following into the resulting choice of components and iterative prototype design. As the goal is to produce a device that simulates the wrist joint, the starting point is an overview of wrist joint mechanics, mainly through an analysis of wrist kinematics.

The contents presented in this chapter are either directly relevant to the production of the final rotary prototype presented in section 3.3, or contributed in some significant way to justify the approach towards its design. As such, and due to the exploratory nature of this work, some of the contents presented in this chapter were not utilised in the final version of the prototype due to limitations in the methods chosen for their implementation, and not in terms of their general validity for a future application.

3.1 Theoretical Fundamentals

3.1.1 Wrist Joint Mechanics

In the context of kinematics, the wrist joint can be described as a spherical actuator, as it is able to move in two axes of rotation around its center. A wrist flexion is performed by rotating the hand towards the forearm in the direction of the palm, whereas the opposite movement is called an extension. An example of such a movement is represented in figure 2.2, with the larger arrow indicating the direction of an extension. The iHandU wearable device only takes into consideration the wrist flexion movement when performing its assessment [4].

In order to create a simulator capable of producing a rotational actuation, we may use the rotational properties of aforementioned components such as electric motors or MR brakes. An example could be to fixate an actuator of this type to a surface, then attaching a lever-like, hand-shaped structure to it, as discussed in section 2.4.1. In this case, however, we are simulating a wrist, and as such we wish for the measurement of the lever length to be within reason of that of a human hand, and for the user to be able to hold the hand-like structure in a generally comfortable manner.

Actuation of the chosen component, whether passive or active, can then be electronically controlled by a microprocessor to respond to the system inputs and chosen parameters.

The other axis of movement in the wrist controls adduction and abduction, and while its inclusion could result in a more versatile and lifelike final product, it also carries the weight of an increased complexity on both the structural and actuation level that may prove ultimately unnecessary.

Spherical actuator designs exist [20], although developing one for this purpose would be a lengthy and time-consuming process, considering that the addition of a second axis is not a requirement, and would be done only for the sake of future versatility. Interestingly, an open-source, 3D-printable wrist-like spherical actuator solution exists as part of the simulator *Parloma* [18]. It represents a novel endeavor to enable remote communication among deaf-blind people, based on the similarly open-source, human sized 3D-printable robot, InMoov [9]. Most importantly in this context, all custom part files are made freely available by the developers in the project's *Thingiverse* page [1], and thus available for rapid prototyping through 3D-printing. Given this resource, the first prototype was based on this printable structure.

3.1.2 Electric Motors and Dynamic Braking

Electric motors are a widespread type of electrical machine, capable of converting electrical energy into mechanical energy. A variety of electric motor types exist, generally operating through use of electromagnetic induction in order to produce a motor torque from a given electric input. As is common in energy conversion, the efficiency of this process is not perfect, and is therefore subject to losses. In electric motors we verify both electrical losses, such as rotor resistance losses, and mechanical losses, such as friction.

In emulating the wrist joint, we would be using a single motor to control the flexion and extension movements, performed on the same axis but different directions. We will focus on permanent magnet DC motors, as their performance is typically independent of their sense of rotation [7]. A simplified representation of this type of motor is visible in figure 3.1, but the exact component configuration may change depending on the manufacturer.

In this type of motor, mechanical power is generated by running an electric current through a set of motor windings in the rotor through contact with a set of brushes. This induces a magnetic field, according to *Faraday's Law of Induction*, that causes the windings to be repelled by the motor permanent magnets. In turn, this causes the rotor to spin, producing a mechanical torque in the output shaft [7].

As the coil moves in this way to a position perpendicular to the magnetic flux, the resulting torque will approach zero. At this point, in the case from figure 3.1, the brushes would connect to the opposite coil terminal, reversing the direction of the magnetic field, and the aforementioned repulsive interaction would repeat. However, this large oscillation in the magnetic repulsion causes

[1] https://www.thingiverse.com/thing:1597390

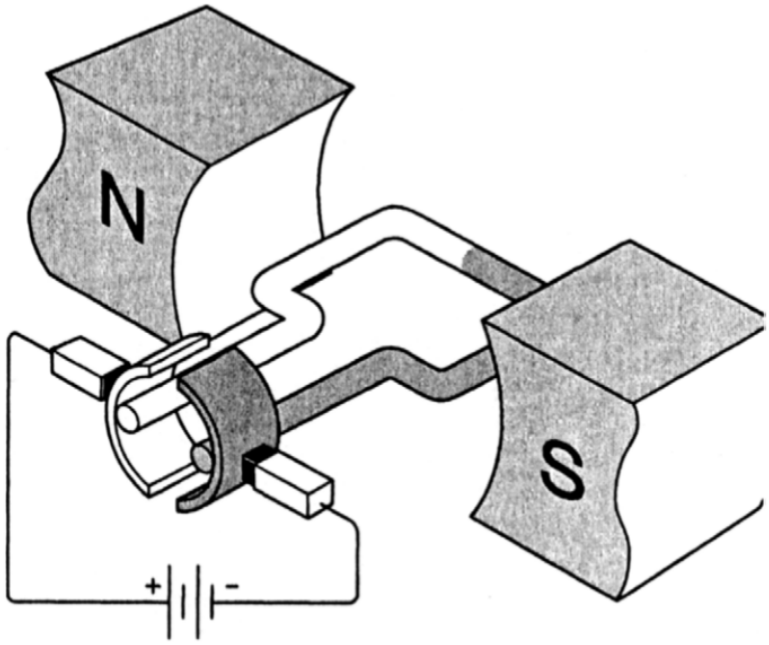

Figure 3.1: Diagram of an electric motor. Extracted from [7], pg.25

a large oscillation in the mechanical torque output. For this reason, typically, additional sets of windings are employed in order to achieve a more uniform mechanical behavior.

By applying an external torque to the motor shaft, a magnetic field variation will appear through the motor windings, due to the magnetic flux of the permanent magnets. Due to this, conversely to its normal operation, a voltage will be produced on the motor electric terminals as a result of a mechanical action in the motor shaft. In this way, such an electric motor could be used as a generator, converting mechanical power into electric power.

Dynamic braking refers to the braking effect that is verified when a coasting motor's electrical terminals are short-circuited, or connected to a sufficiently small load. Represented in figure 3.2 is a typical setup for such an application. What follows is a description of this phenomenon.

In the case of a DC brushed motor, let us consider the simplified diagram in figure 3.3. In this diagram, the electrical losses are abstracted from an *"ideal"* motor. As such, the input voltage v_i will be distributed between the motor's internal resistance R and the motor winding voltage e_v, resulting in a current i. As a result, the motor shaft will generate a torque, $\tau(Nm)$ [1].

If the motor is rotating at an angular velocity $\omega(rad/s)$, a varying magnetic field appears through the center of the rotor windings, and the motor will function as a generator, as previously mentioned, inducing an electric current in the rotor windings [1].

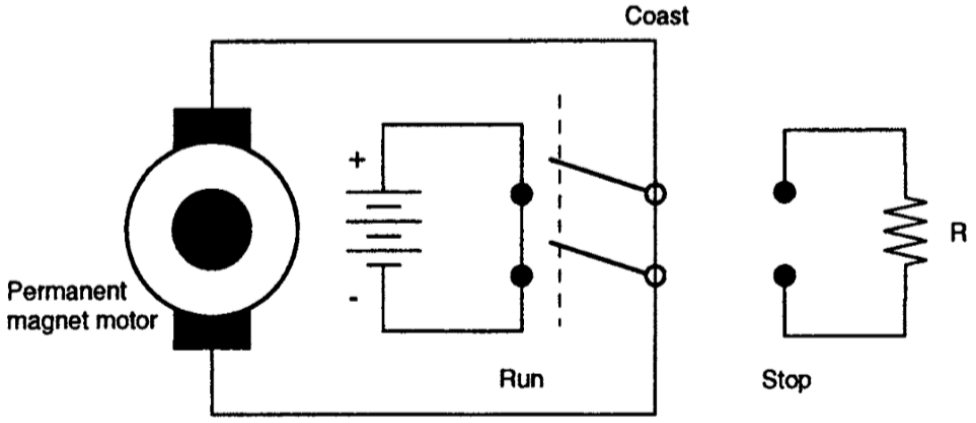

Figure 3.2: Example setup for dynamic braking of a DC motor, extracted from [7], pg.116

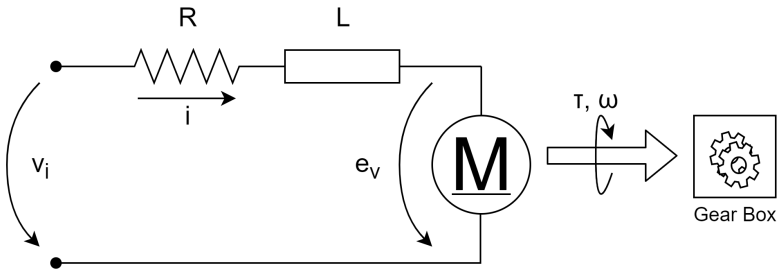

Figure 3.3: Simplified motor RL diagram

Considering the effect of L as negligible and the motor constants $K_t = K_e = K$, let us consider the following motor equations [1].

$$v_i = R \cdot i + e_v \tag{3.1}$$

$$\tau = K \cdot i \tag{3.2}$$

$$e_v = K \cdot \omega \tag{3.3}$$

If the motor terminals are connected by a small electric load or even short circuited, so that v_i is negligible, we obtain:

$$i = \frac{-K \cdot \omega}{R} \tag{3.4}$$

The electric current generated in this way will provide a torque, $\tau(Nm)$, opposite to the direction of angular velocity, as seen in 3.2. This effect is typically capable of rapidly braking this type of motor, and Alternatively, by regulating v_i, we instead obtain the following property from 3.1, 3.2 and 3.3:

$$\tau = \frac{K}{R} \cdot v_i - \frac{K^2}{R} \cdot \omega \tag{3.5}$$

From these properties, the idea arose to control this effect by using Pulse Width Modulation (*PWM*), using an adequate transistor as an electronic switch, in order to use the motor as a passive brake-like component to be applied to the simulator joint. As described in section 2.4, a passive actuation method would provide a safer alternative in the event of an electrical or control malfunction.

The material concerning dynamic braking that was reviewed in this section was ultimately not utilised in the final version of the prototype, however it is retained in this work as it was a significant factor in the choice of an actuation method. Furthermore, this section provides information that can be of use in the future to provide a passive, safer method of actuation for the simulator.

3.2 Spherical Actuator Prototype

The human wrist joint motion can be described by two rotational axes - one for flexion and extension, as represented in figure 2.2, and another for adduction and abduction, for motions parallel to the palm of the hand.

The movement axis for adduction and abduction is not necessary to simulate the intended exercise. However, in the context of a complete simulator, the use of a spherical actuator would result in a more versatile end result that could potentially be adapted to variations of the wrist rigidity assessment motions described in section 2.2. Due to this, and also due to the availability of an adequate structural candidate, this first prototype constitutes an attempt to create a full wrist simulator.

The aforementioned candidate for a spherical actuator was identified in the Parloma [18] wrist. a 3D printable robotic hand and wrist designed to allow remote communication between deaf-blind people, itself a modification to the InMoov open-source 3D printable life-size robot [9].

Given this resource, a prototype was 3D-printed and promptly assembled, as shown in figure 3.4. Test actuation was performed using MG90 servomotors controlled by an Arduino Uno using PWM, with plans for a proper control strategy through application of forward and inverse kinematics in order to produce the intended response.

However, a preliminary assessment of the assembly results found the prototype structure to be unsatisfactory – even after extensive exfoliation and oiling of the moving parts, its movements were noticeably coarse. Furthermore, small movements of the central shaft caused it to move out of range of the actuator gears leading to gear slipping, and standard operation caused some of the joints to come loose. These problems, coupled with the already nontrivial control of this structure, resulted in an imprecise and unreliable structure that would be difficult to elevate to a working state, thus unsuitable for this application.

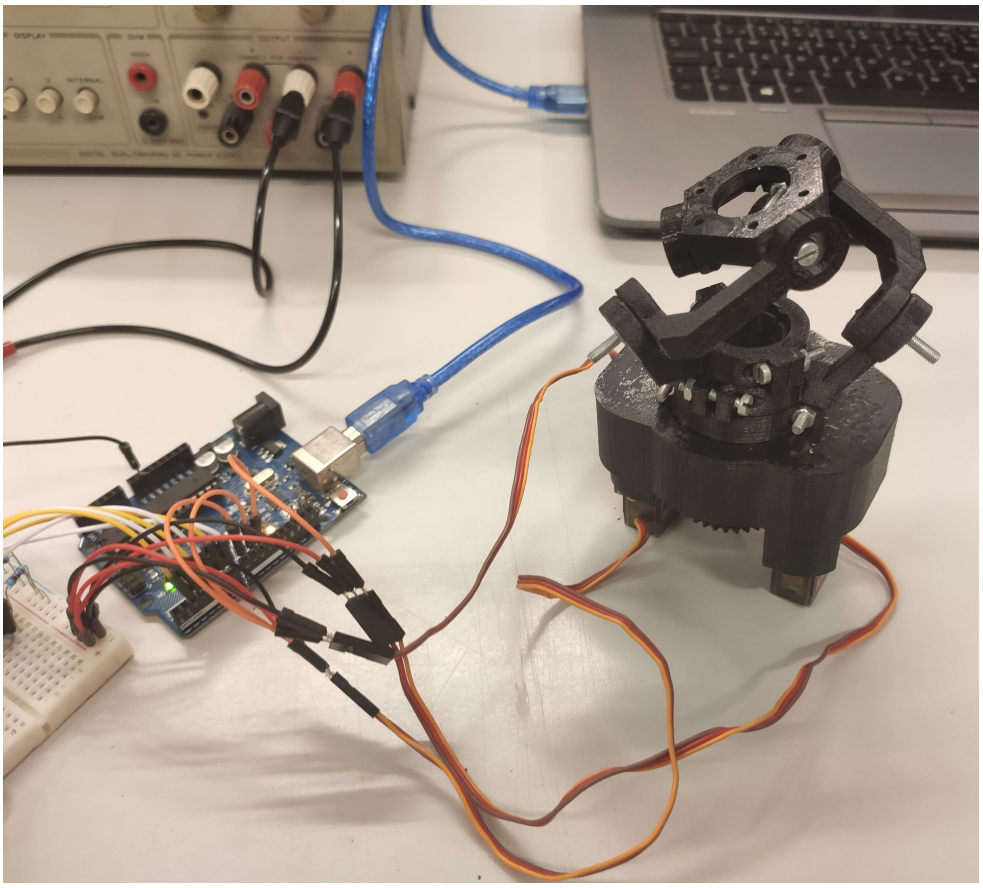

Figure 3.4: 3D-printed spherical actuator

Nevertheless, this approach could be viable by using a more precise printing method, different materials or even a structural redesign, however these would likely imply either a greater cost, a large time expenditure, or both.

Here, the decision was made to opt for a simpler, more robust model, as although an adduction/abduction axis could make the simulator adaptable to other rigidity assessment exercises, the time investment needed to improve or create one such structure locally did not justify the end result, as this axis is not necessary to perform the rigidity assessment and is not required by the iHandU.

3.3 Rotary Actuator Prototype

Considering that the exercise to be simulated relies predominantly on the flexion and extension of the wrist joint, the next approach focuses on producing a simulator with a single rotation axis, effectively trivializing the structure kinematics, as a single actuation axis can be responsible for regulating the mechanical impedance in the rotary wrist by application of a variable torque.

In other words, the goal here is to produce a wrist-like mechanical structure with one degree of freedom by fixating a hand-like structure to the output of a rotary actuator. Considering the

analysis performed in sections 2.4.2, and 3.1.2, a commercial brushed DC motor shall be selected in section 3.3.1 for this task.

Since the information present in most motor data sheets is insufficient to categorize the dynamic braking response such as gear box losses, it is possible that the dynamic braking effect produced by the chosen motor alone will not be capable of adequately modeling wrist rigidity. In such an event, a commercial H bridge circuit shall be selected in order to actively power the motor in the intended direction. For passive use of dynamic braking, an adequate transistor would be chosen and operated as a switch, controlled via PWM to provide the desired motor response.

On the subject of control, in order to facilitate the development and prototyping of higher-order systems and nonlinear response mechanisms, a microcontroller-based programmable solution would be very convenient. A control approach is necessary due to the nature of the problem, as the same force will not be applied by all clinicians during the rigidity assessment and simple system parameter variation is a requirement. Here, some form of force sensing must be considered.

Force sensors such as strain gauges have been previously mentioned in section 2.4.2. This type of sensor would serve to generate a control signal to be applied to the actuator in order to produce a suitable response. The current development cycle of the iHandU integrates resistive force sensors in the textile band in order to measure the force applied by clinicians. These pad-like sensors are lightweight and relatively small.

However, in the context of a mechatronic simulator, an arguably better option exists in *load cells*. These are larger sensors that employ strain gauges to measure typically minute distortions on a structure such as a metallic bar, as the structure is slightly bent with the application of force on its extremities. This allows for the extraction of weight measurements through analysis of the strain gauges' resulting output voltages. Advantages in the use of a load cell include a sturdier body, the measurement of forces over a larger surface area and the measurement of forces in positive and negative directions, for bar-shaped load cells. A convenient solution for our application is here envisioned by connecting a load cell to the motor shaft in a way that provides a lever-like structure with the ability to perform reliable force measurements. The other load cell extremity may then be sheathed in a hand-like grip for user comfort and anatomic similarity purposes.

Finally, in order to regulate position-based nonlinearities, such as cogwheel rigidity and the maximum flexion and extension angles of the wrist, a device such as a rotary encoder may be attached to the motor in order to obtain accurate and reliable position data for the hand-like segment.

Given these conditions, the regulation of the motor torque according to the input force on the load cell will be performed as depicted on figure 3.5.

The logging of output data will require a gyroscope similar to the one present in the iHandU, for data comparison. Additionally, a rotary encoder would certainly prove useful as a stable measurement of the joint's current angular position.

With this configuration, the use of custom design parts is very limited, comparatively to the simulators seen in section 2.4, in that we require only a hand-like structure to attach to the load cell extremity, a steel link to connect the DC motor shaft to the load cell, and some base with which to fixate the motor and electrical components.

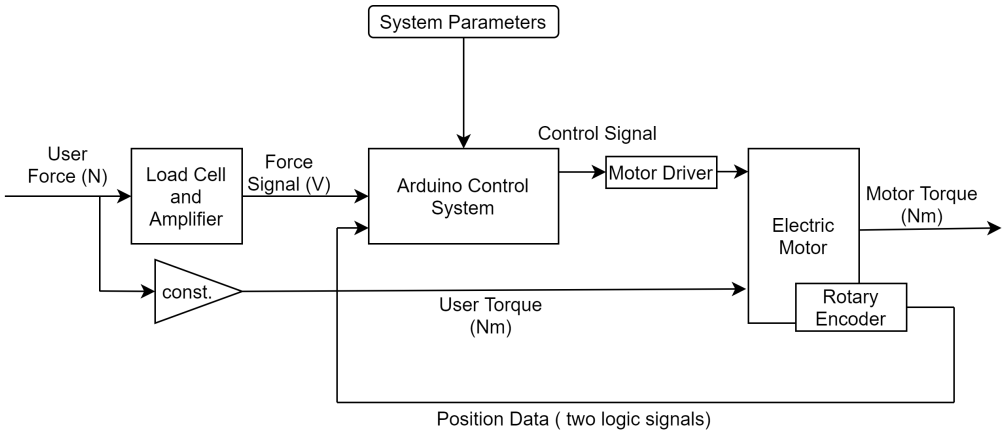

Figure 3.5: System input-output block diagram. A detailed view of the Arduino Control System block is later presented in figure 3.14. The depicted gain constant relating force and torque refers to the length of the hand-like segment.

The following subsections will focus on the selection of suitable components as per the previously outlined guidelines.

3.3.1 Commercial Component Selection

Most of the components we will require have a suitable array of commercial solutions readily available at most specialized retailers.

The *Arduino Uno* constitutes a simple, programmable electronic prototyping board, based on the Atmel ATmega328 microcontroller. It is compatible with a wide range of sensors and actuators, being equipped with several digital and ADC ports, pull-up resistors and I^2C communication support. It is also capable of sending data to another machine in real time for data logging and display purposes through its USB type-B serial port, which will also be used to power the Arduino and most sensors connected to it. As its characteristics and versatility meet our needs, it was chosen as the central electronic module for our system, and is responsible for controlling the actuator based on the obtained sensor data.

Concerning actuation, the Robot Electronics *EMG series* of permanent magnet brushed DC motors stood out due to its ease of availability, relatively low price point and inclusion of an integrated encoder as well as a planetary gear box. The planetary, or epicyclic structure in a gear box allows for conventional gear reductions while distributing the force of these reductions in several planetary gears, which helps to prevent gear fractures and slipping. A diagram is featured in figure 3.6 A compatible aluminum mounting bracket exists for these motor models as well, and enables simple fixation of the motor to an even surface or base.

Data sheet information does not present sufficient information to exactly determine the dynamic braking response, especially taking into consideration factors such as mechanical losses in

[2] https://www.instructables.com/id/Planetary-Gear/

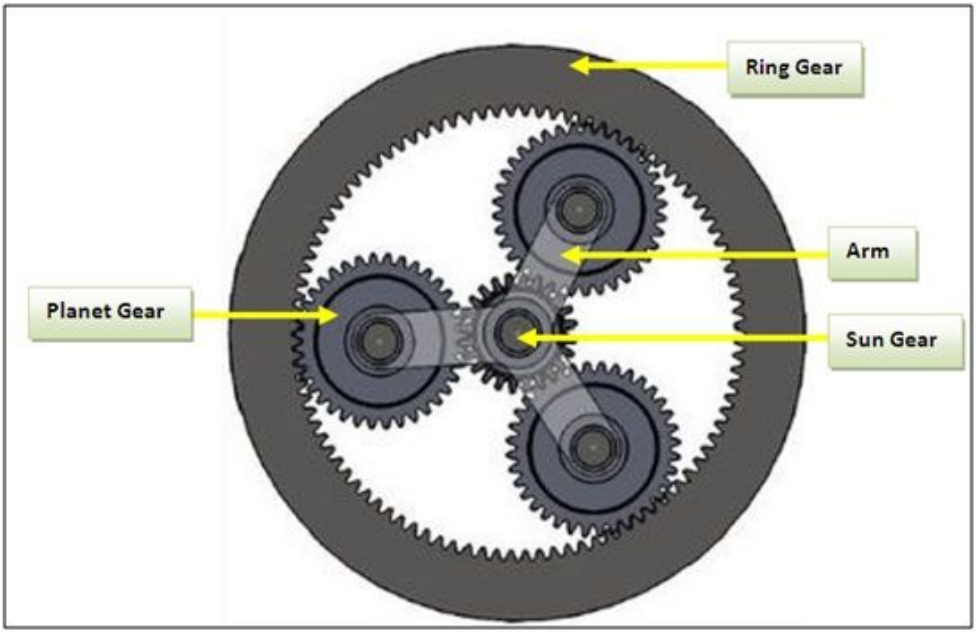

Figure 3.6: Diagram of an epicyclic gearing setup. Source[2]

the gear box. As such, the EMG49 [3] model was selected over the EMG30 due to its much higher stall current and rated voltage (13A, 24V), since in the event that dynamic braking is not utilised, the motor will be instead used as an active component while stalled by an external torque in normal operation. The aforementioned corresponding mounting bracket was acquired as well.

During preliminary testing, it became clear that the motor base mechanical impedance due to gear box attrition was too elevated to simulate a wrist at the best percentage of rigidity improvement. For this reason, a compatible VNH3SP30 H bridge motor driver was integrated in the simulator to allow for control over the electric power provided to the motor through an appropriate regulated DC power source. The role of each component in converting the input force into an output for this case is later detailed in figure 3.5 The dynamic braking approach can be experimented on in the future by testing different motors or replacing the included 49:1 gear box with a modular planetary gear box.

The encoder included with the EMG49 presents a resolution of 980 counts per output shaft rotation, meaning that our angular position quantum, the smallest measurable movement, will be of approximately 0.0064 rad, which is ostensibly an adequate value for this application.

Concerning the weight sensor, an *HY-1B 50Kg Load Cell* was selected. This load cell is rated to sense weights of up to 50Kg on either orientation, and measures approximately 106mm in length from the approximate placement of the motor shaft to the region of force application, as shown in figure 3.7. Observations indicate that the load cell length is within reason, albeit leading to a result slightly longer than an average hand. The full range of the load cell is not expected to be fully utilised during a reasonable rigidity assessment exercise. This device was selected due

[3] https://www.robot-electronics.co.uk/htm/emg49.htm

to temporary unavailability of other options, but is nevertheless suitable for this application as it presents adequate characteristics at a similar price point.

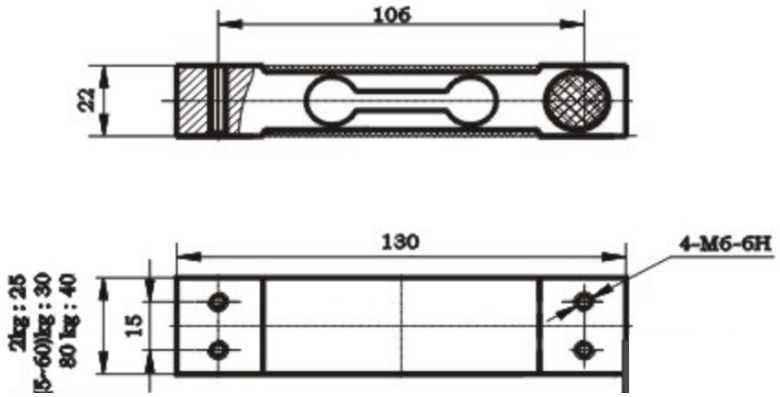

Figure 3.7: HY-1B 50Kg Load Cell diagram extracted from [4]

In order to facilitate force readings from the load cell strain gauge differential outputs, an *HX711 load cell amplifier*[5] was used. This is an integrated circuit based on the Avia Semiconductors HX711 ADC for weight scales, used in order to obtain periodic weight data from the load cell through synchronous communications at a rate of up to 80 samples per second.

After programming, the simulator should now be capable of controlling the motor torque in accordance with its current relative position, as well as the force applied to the extremity of the load cell. Data communication may be handled by the Arduino Uno via serial port as a means for external data logging through a generic compatible device. However, since we wish to compare the obtained data to that of the iHandU, we also require an adequate reading for angular velocity. Such a reading would also be useful for a future implementation of a higher-order rigidity/viscosity model.

It is true that a measure of angular velocity may be obtained by differentiating the encoder signal. However, we can quickly demonstrate that such an approach would be undesirable through data sheet analysis, as the encoder is rated at 980 counts per output shaft rotation, whereas the HX711 will provide a new load cell reading at a frequency of approximately 80 Hz, limiting the frequency of our control loop. At this frequency, the quantum of our differentiated angular acceleration will be approximately 0.5129 radians per second, as shown below in 3.6.

$$q = \frac{2\pi}{counts\ per\ rotation} \cdot f = \frac{2\pi}{980} \cdot 80Hz \approx 0.5129\ rad/s \tag{3.6}$$

This result was later verified to some extent, during the gyroscope calibration in section 3.3.3. This value could be reduced by using a slower cycle frequency. This would be detrimental to the

[4] https://www.botnroll.com/index.php?id_product=967&controller=product&id_lang=7
[5] https://cdn.sparkfun.com/datasheets/Sensors/ForceFlex/hx711_english.pdf

system's main application as it would imply an unnecessary actuator delay by slowing down the control loop, which could lead to system instability.

For this reason, the *SparkFun IMU Breakout*[6] was selected, due to its immediate availability in the BRAIN laboratory allied to its suitable characteristics, such as a gyroscope legible through a 16-bit ADC, with a scale range of up to ±2000 degrees per second. This is a breakout board based on the InvenSense MPU-9250 IC. This breakout board is capable of providing accelerometer, gyroscope and magnetometer readings, which are legible via I^2C serial communications. It is also equipped with an interrupt pin to inform the I^2C master when all values have been updated, but it is not fully used in this project as both Arduino Uno Interrupt Service Routine (*ISR*) ports, digital ports 2 and 3, have been reserved for use with the EMG49 encoder. This is necessary in order to utilize the device's full resolution in a way that will be detailed in section 3.3.4

3.3.2 Custom Component Design and Production

Suitable, cost-effective commercial components were found for all needed sensing and actuation applications. However, concerning the structure, there is the need for two mechanical components with specific designs, as well as a generic base to house the simulator structure and electronic components.

A component with sufficiently high mechanical resistance is needed to anchor the motor-side load cell to the motor shaft. Additionally, a hand-like structure with which to guard the user-side load cell extremity would provide additional comfort and realism to the user.

The **link** between the load cell and motor shaft was designed using readily available component data sheet measurements for the motor and load cell, and produced in steel at the Faculdade de Engenharia da Universidade do Porto (*FEUP)* Mechanical Engineering department workshop (*DEMec*). For the purpose of simplicity, this design consisted in a simple cuboid shape with appropriately sized indentations and perforations to house the load cell and motor shaft, and fixate them using appropriately sized bolts. The resulting structure is displayed in figure 3.8.

The **hand-like structure** was designed using SolidWorks 2019 Student Edition software provided by Faculdade de Engenharia da Universidade do Porto. It was designed to resemble a closed human fist, based on observational accounts of rigidity assessments performed at Centro Hospitalar de São João, which described that the assessment was carried out while the patient's hand was held in a fist, along the length of the proximal phalanxes.

This part was designed for 3D printing in Polylactic Acid (*PLA*). Emphasis was placed on structural integrity and comfort, while using reasonable dimensions for the structure, based on those of an actual human hand: 80mm in breadth, 60mm in height or length of the proximal phalanxes, and 60mm in segment length as it was sufficient to adequately cover the load cell. All user-side corners were rounded for comfort, and the matching internal corners were rounded as well in order to prevent the creation of structural weak points. This component's thinnest segment

[6] https://www.sparkfun.com/products/13762

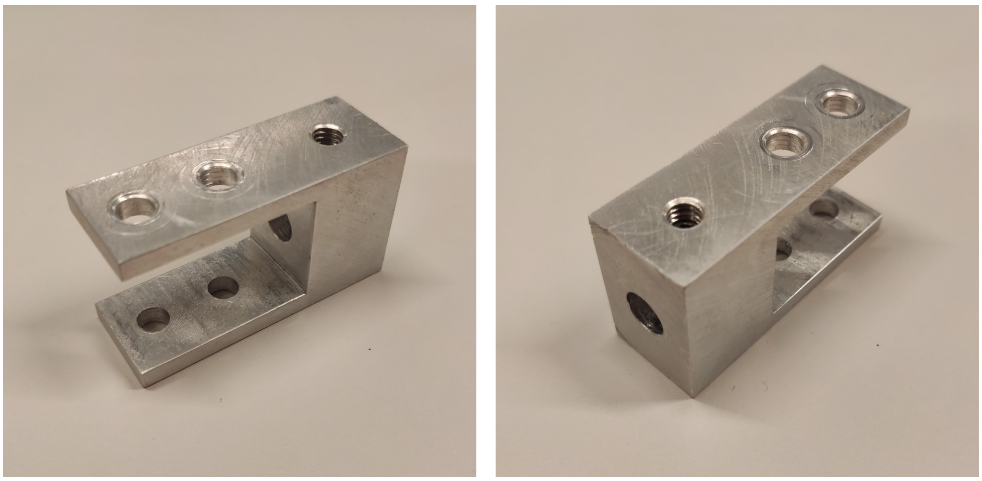

Figure 3.8: Custom link to connect the load cell and motor shaft

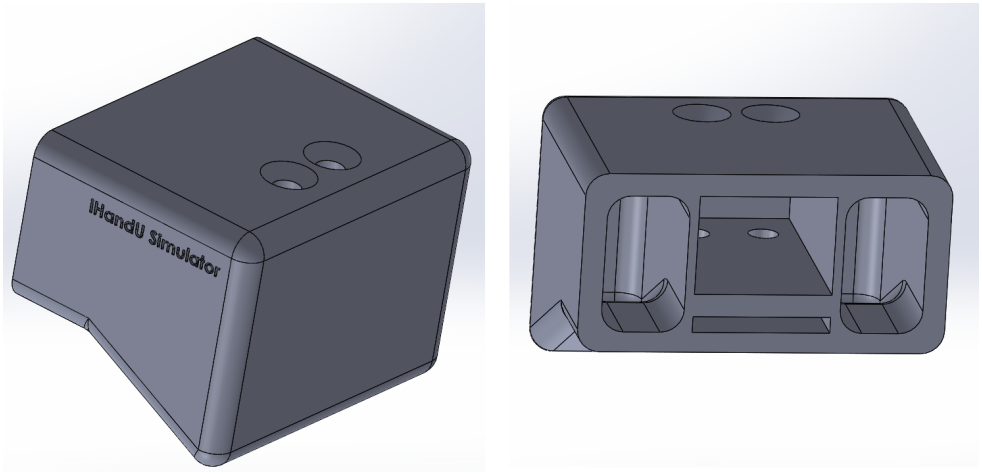

Figure 3.9: SolidWorks representation of the simulator fist-like extremity

is to the left and right of the visible load cell slot in figure 3.9, with a width of 0.2 cm in its thinnest section.

The base used for the simulator is a wooden slate with a thickness of 0.5cm on the underside of which small alcoves were drilled as housings for the underside of the bolts used to fixate the aluminum motor support structure while retaining a flat underside.

By assembling the simulator components as described, we obtain the final structural result visible in figure 3.10.

In this configuration, sensor and actuator rotation directions were set according to their specifications and confirmed experimentally. The resulting conventions are described in the following diagram 3.11.

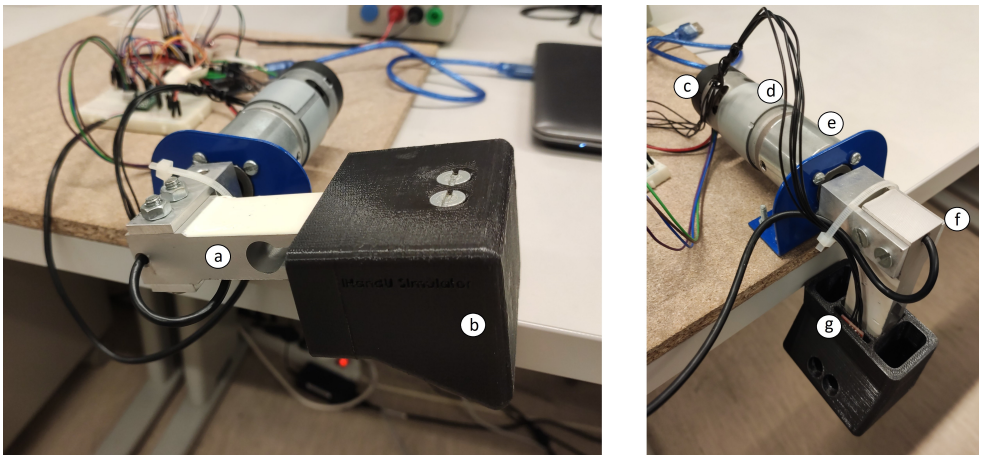

Figure 3.10: Mechanical setup of the wrist rigidity simulator. The represented parts are as follows. a) load cell; b) fist-like structure; c) EMG49 encoder; d) EMG49 electric motor; e) EMG49 gear box and mounting bracket; f) custom steel link securing the load cell to the motor shaft; g) MPU-9250 motion sensing breakout board

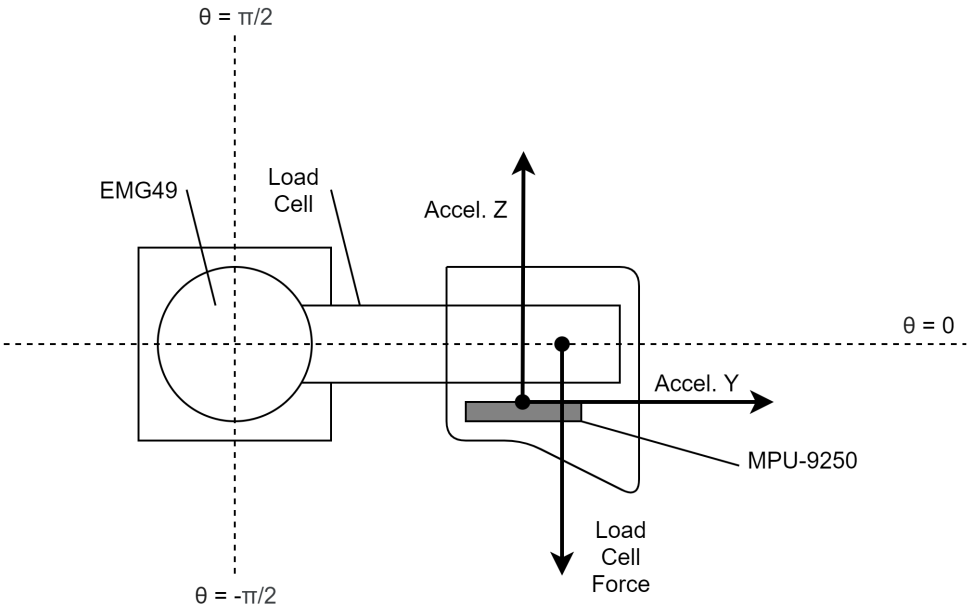

Figure 3.11: Rigidity simulator schematic and directional conventions.
Arrows indicate the positive sense of the measurement. Motor torque and encoder measurements are positive in the positive sense of θ. Gyroscope X-axis angular velocity measurements are negative in this sense.

3.3.3 Sensor Setup and Calibration

All sensors used in this project are powered by, and report their respective data to the *Arduino Uno*, through several methods described below. This data is then received and analysed through USB port serial communications with a compatible device, in this case a personal computer.

The *EMG49 encoder* outputs are two open-collector transistors, requiring pull-up resistors to the desired output signal, between 3.5V and 20V. The two encoder channels were connected to Arduino Uno ports 2 and 3, and the on-board 5V pull-up resistors were enabled for these pins. These pins were selected so that interrupt service routines (*ISR*) may be used to take advantage of the full resolution of the encoder in a way detailed in section 3.3.4. No further encoder calibration is required due to the nature of the device.

The selected *HY-1B 50Kg Load Cell* was connected to the *HX711 Load Cell Amplifier*, in turn connected to the *Arduino Uno*. The load cell amplifier sends data synchronously by using the DAT and CLK pins. For convenience, this interaction is handled by the open-source HX711 Arduino Library v0.7.2 by Bogdan Necula [7].

While calibrating the load cell, we must mind the fact that the gravitational force on the extremity of the load cell will vary with its inclination θ, according to the simple property below, where k represents the weight measurement read when the mounted load cell is parallel to the ground with no load in its extremity:

$$F_g(\theta) \quad = \quad k \cdot cos(\theta) \tag{3.7}$$

First, the load cell gain was calibrated with the arm in the horizontal position, where F_g is maximal. This position was defined as zero with no load, and the readings were compared to known weights. The scale gain for conversion into newtons was thus determined to be approximately 8000. Then, the arm was rotated to be perpendicular to the ground, where the effect of F_g would be negligible, giving us the actual offset value in the order of -44600 units. The value of k is then trivially obtained by rotating the arm back to the horizontal position with no load, and determined to be around 0.95N. This procedure must be repeated if any significant modifications are made to the fist-like load cell extremity. Through use of this property, we can estimate the gravitational force component detected by knowing the value of θ, and subtract it from the load cell reading to estimate the user-applied force

The *MPU-9250 breakout board* is equipped with an accelerometer, gyroscope, magnetometer and internal thermal sensor, being that the latter two are not of interest for this project and will not be used. Concerning power, the board requires 3.5V on its *VDD* pin, and pull-up resistors for the I^2C communication pins *SDA* and *SCL*.

Concerning the *MPU-9250 accelerometer*, we know that while the device is in a fixed position, the acceleration direction vector will sensibly correspond to the gravitational acceleration. Reminding that the accelerometer is secured underneath the hand-like structure parallel to the load cell, and referring to the diagram presented in figure 3.11, we proceeded to slowly rotate the motor in key areas in order to obtain offset and gain values for the Y and Z axis. The accelerometer X axis is unused, as it will always point in the same direction, parallel to the ground. A quick verification was performed by verifying that while joint movement is halted the modulus of the

[7] https://github.com/bogde/HX711

acceleration vector sensibly corresponds to the gravitational acceleration vector with a value of $9.8m/s^2$.

Regarding the *MPU-9250 gyroscope*, its measurement of rotational velocity is difficult to calibrate in a similar way. By resorting to data sheet information, namely the device scale and range (2000 degrees per second, 16-bit ADC), we were capable of calibrating the X axis measurements, and verifying the accuracy of this calibration through comparison with the lower precision encoder derivative, as shown in figure 3.12 with satisfactory results.

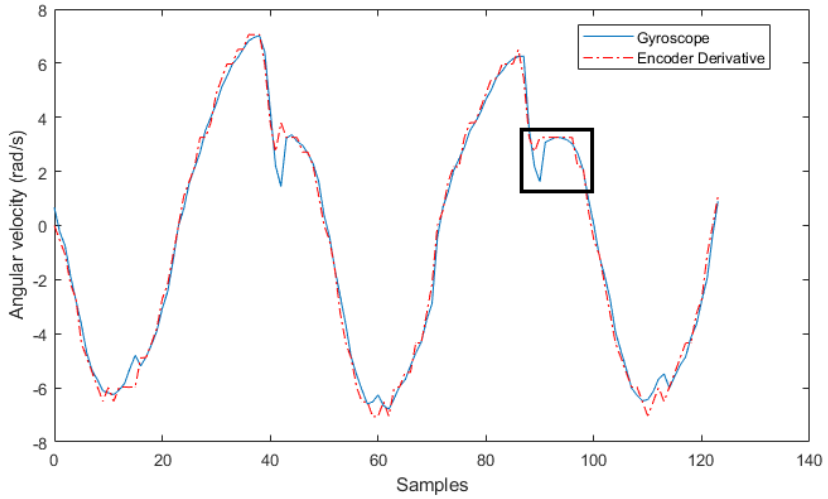

Figure 3.12: Comparison of the gyroscope output and the result of encoder derivation. The black square denotes the region shown in figure 3.13

From this figure, we are capable of observing that the gyroscope values are reasonable, when compared to the known encoder derivative, which provides an accurate yet rough signal due to the high signal quantum of around 0.5 radians, as seen in property 3.6. This is further explicited in figure 3.13. The gyroscope readings were also later compared to those obtained from the current version of the iHandU during the results discussion, in chapter 4.

3.3.4 Model Definition

The program run in this simulator can be divided in two principal functions, much like a typical Arduino program: the **setup**, where system variables are defined, scales are calibrated (as discussed in the previous section) and device parameters are set, and a control **loop**, where the program runs cyclically, receiving sensor readings, controlling outputs and transmitting process data as required. For simplicity, the firmware was programmed in the official *Arduino IDE*. Data sent by the Arduino through serial communications may be roughly visualized using the *IDE* serial plotter, or exported to another software such as MATLAB for a detailed analysis.

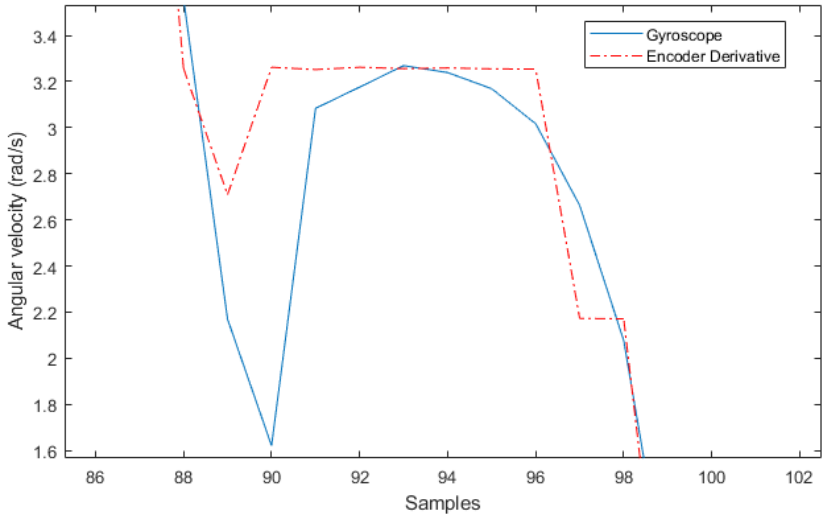

Figure 3.13: Closer look at the comparison of the gyroscope output and the result of encoder derivation. Here we can observe the rougher quantization of the encoder derivative as deduced from property 3.6.

A general diagram of the process model can be found in figure 3.14, where we regulate an electrical motor torque as a result of the user force and the system state. The motor in its unpowered state already presents an intermediate level of rigidity due to gear box attrition. For this reason, the control signal sent to the motor may be assistive or resistive in relation to the user force, depending on the system parameters.

Now that the simulator structure has been assembled and sensor scales have been calibrated in order to obtain correct sensor readings, we must define the command structure used in order to generate the control signal applied to the motor. A diagram of this structure can be found in figure 3.14, and an explanation of each function and system parameter will be given shortly. This section features several operations which are to be executed on each Arduino cycle. As such, care was taken in conserving memory availability through sensible allocation of process variables and avoiding the use of methods with a long execution time, bearing in mind that the Arduino Uno has a relatively limited memory and processing power.

In order to deliver a smooth system response, there was a need to further filter the amplified signal beyond the filter applied by the IC itself. For this reason, and since the natural oscillation frequency produced by the exercise differs with the practitioner and may not even be constant, a digital second-order butterworth low-pass filter was selected, with a cutoff frequency of 3Hz, in order to attenuate signal noise while retaining a flatter pass-band. Using this filtered output, a variable gain is applied in order to produce a control signal that can be sent to the motor driver in order to regulate the joint mechanical impedance. This gain, in turn, is regulated by the *rigidity %* parameter, as shown in figure 3.14.

From this filtered load cell output, we are capable of estimating the force applied by the user,

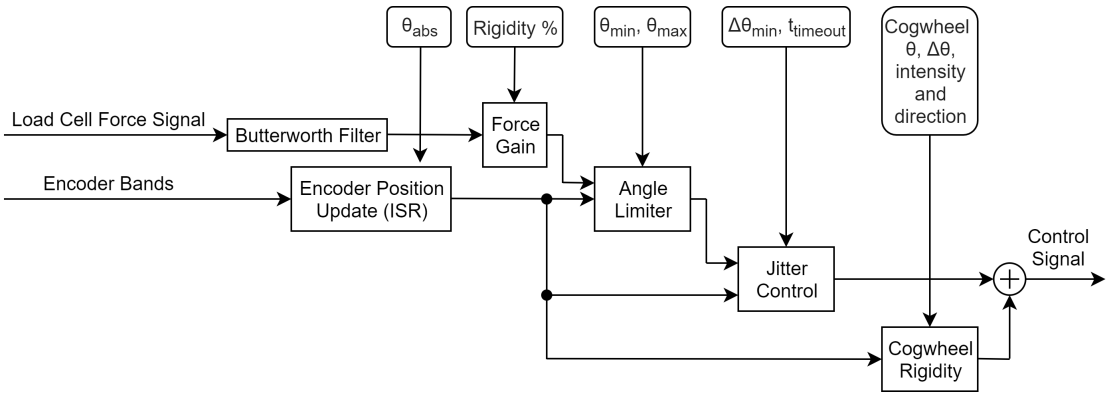

Figure 3.14: Generation of a control signal from the sensor signals (left) and system parameters (top).

since we can obtain an approximation of the force exerted by the load cell's own weight through the property in 3.7. In the current case, we allow the system to react to this force like any other, just as a passive human hand tends to hang limp. However, the potential to modify this behavior in a future model exists.

A rotary encoder, such as the one present in the EMG49, is a device capable of detecting small relative angular movements applied to its axis. In this case, the encoder is integrated in the EMG49 and attached to the back of the motor, in the opposite end to its shaft. This encoder outputs data through two open-collector hall sensors that detect the rotation of an internal component. These hall sensor channels provide logical outputs similar to square waves, which are 90º out of phase from each other in a way that allows us to determine the direction of rotation by observing the channels' state when a rising or falling edge occurs in either band, as shown in figure 3.15.

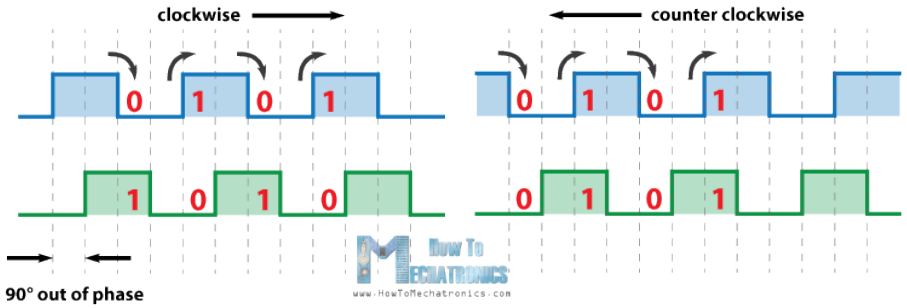

Figure 3.15: Understanding encoder rotation direction from band signals. Source [8]

In order to do this, and thus use the full encoder resolution, the logical signal variations in both bands must be detected, and subsequently the position counter must be incremented, even if they occur while our microprocessor would be otherwise busy. Therefore, each encoder band hall sensor output was connected to one of the Arduino Uno Interrupt Service Routine (*ISR*) pins,

[8] https://howtomechatronics.com/tutorials/arduino/rotary-encoder-works-use-arduino/

namely pins 2 and 3, while also activating these pins' internal pull-up resistors in order to properly read the hall sensor open collector outputs. Additionally, the angular position variable used should be declared with the *volatile* qualifier, since its value may change at any time.

Two ISRs were used, each attached to one of the logic signals. Whenever a signal changes its value, its respective ISR is triggered, calling a function that detects the direction of the angular movement that just occurred by reading both bands' data. As an example, and referring to figure 3.15, let us consider the top band as channel A and the bottom band as channel B. If the channel A ISR is triggered and the value of A is not equal to the value of B, we will know that the device has rotated clockwise. If A and B are equal in this moment, then the device has rotated counter-clockwise. As a result, the position counter is incremented or decremented accordingly. A similar action is performed if the channel B ISR is triggered.

Through use of the encoder alone, this provides only a relative measurement of angular position, meaning that a fixed starting position would need to be defined. However, using the accelerometer present in the MPU-9250 breakout board, we are able to compute the hand segment angular position in the device starting sequence. When the device rests undisturbed, the accelerometer direction vector is equal to the gravitational force exerted on the simulator extremity. Knowing this, the initial angular position is defined through use of inverse trigonometric functions, as exemplified in figure 3.16, and thus we obtain the value of the parameter $\theta_a bs$.

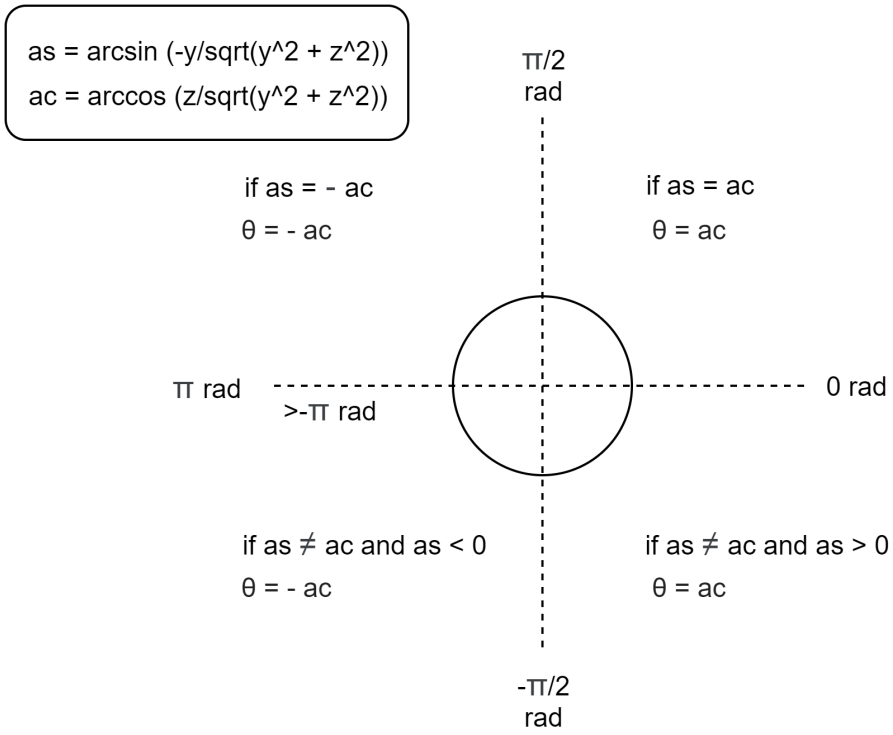

Figure 3.16: Computing the hand segment angle θ using accelerometer y and z axis

Now that we have made available a signal for the absolute angular position of the wrist joint, we are capable of programming several nonlinearities to mimic physical properties of the wrist.

In order to prevent the motor from continually spinning around its axis, were a constant force to be applied to the load cell, the *angle limiter* block was implemented. It receives a maximum and minimum angular position argument, defined in the code, and adds an opposing term to the aforementioned control signal if the force exerted would cause the angular position to exceed the positive or negative limit. This term rapidly increases the further this position is exceeded, creating a similar feeling and intending to produce a slight elastic response, just as when a passive wrist joint is flexed or extended to its limit.

Similarly, we can use the encoder reading to program a motor response similar to *cogwheel rigidity* by reducing or even inverting the control signal in a very small region near the central ($\theta = 0$ *rad*) position. Adjustment of parameters such as cogwheel region position, region amplitude and intensity, as well as directionality (only enabling cogwheel during flexion, for example) this behavior can be adapted accordingly.

At this point in development the system appeared to demonstrate the intended behaviour of variable mechanical impedance, according to observations by BRAIN laboratory members more familiar with the procedure. The *VNHSP30* base input voltage was set to 12V through the regulable power source as a result of one such observation, providing adequate wrist fluidity without over-actuation of the joint which would be verifiable, for example, when a patient attempts to assist in the rigidity assessment instead of remaining in a passive state.

At this point, a problem was identified with the simulator behavior, as during a change in the wrist rotation direction the delay in motor actuation would sometimes result in a force spike in the load cell reading, causing the motor to over-compensate this scenario and rotate against the user's hand, producing a new spike in the reading and repeating this oscillatory behavior until the user's hold on the simulator was released or sufficient force was applied.

In order to prevent this behavior, a simple state machine structure was implemented in order to prevent unintended rapid direction changes without sufficient angular movement in the wrist joint, as detailed in figure 3.17. Simply put, once the joint begins rotating in one direction it must exceed an angular variation of $\pi/6$ rad, defined in the $\Delta\theta_{min}$ parameter, relative to the rotation starting point in order for the system to acknowledge a direction change and power the motor accordingly. This control is allowed to time out after a period of time defined in the parameter $t_{timeout}$ during which no user force is detected. This behavior, of course, is not typically verified in the human wrist, but in the context of performing a normal rigidity assessment, this strategy appears to have resolved the problem in question with no noticeable adverse effects.

We are capable of sending text commands through serial input, enabling the alteration of desired parameters during program execution. Some useful commands implemented in this way enable altering the gain from the load cell to the motor in order to produce different levels of mechanical impedance, as well as enabling or disabling the cogwheel rigidity present in the rotation midpoint. Using this method, any other useful or desired program adjustments can be performed during program execution at will.

The **rigidity assessment** is performed according to the steps detailed in [4]. Noting that our system will use a higher sampling frequency, a simple conversion was made so that the same

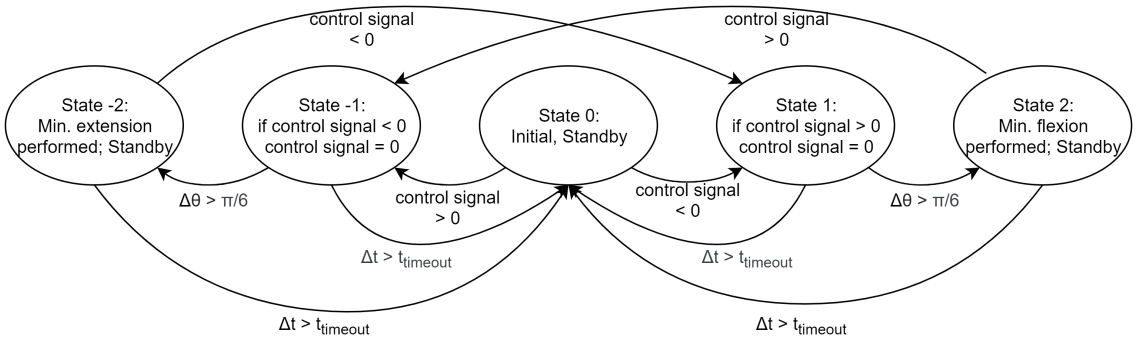

Figure 3.17: State machine approach to control the oscillations verified upon changing direction.

length of time is considered as in the iHandU wearable. In 3.8, from [4], the signal descriptor is calculated from the signal average μ_ω and the average of signal peaks μ_P.

$$\phi = \sqrt{\mu_\omega \cdot \mu_P} \tag{3.8}$$

These values are obtained by setting all gyroscope values lower than zero to zero, as the iHandU only takes into consideration the wrist flexion movement, and then dividing a sum of all signal values and peak values within the assessment period by the number of values read and number of detected non-cogwheel peaks respectively (this detection is performed by obtaining the absolute maximum within each of these positive arcs).

Finally, a rigidity assessment value is obtained through the polynomial function in figure 3.18.

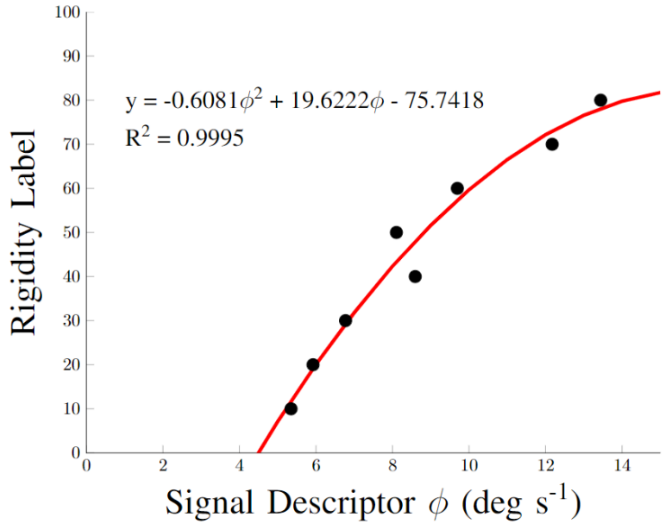

Figure 3.18: Polynomial function used to compute rigidity from the signal descriptor in the iHandU, extracted from [4].

Chapter 4

Results and Discussion

The iHandU simulator resulting from the present work constitutes a wrist-like structure with a fist-shaped extremity, morphologically and functionally similar to a human wrist joint, presenting a comfortable mechanism to simulate a wrist rigidity assessment along a single rotational axis. The current solution dimensions were observationally found to be similar to those of a large, but reasonably-sized human hand. The morphology of the simulator can be found in figure 3.10.

The components necessary to the production of this device, or components similar to those used, are widely available in several specialized retailers. Only three custom components were manufactured, these being the steel link between the motor shaft and the load cell, the hand-like load cell cover and the device base. Of these three methods, production of a new base is a trivial matter, requiring only a generic penetrable slate of adequate material, and the hand-like cover can be replicated easily through 3D-printing. The steel link cannot be obtained through 3D-printing with PLA due to mechanical resistance constraints, however a sufficiently sturdy connective element is needed between the load cell and the motor shaft. In this way, we can conclude that the device adequately satisfies the need for easy replicability.

In relation to the production cost of the device, the retail costs of acquired components, namely the load cell[1], load cell amplifier[2], DC motor, gearbox and encoder[3], mounting bracket[4] and MPU-9250 motion sensing device[5], and the estimated costs of previously owned components such as the Arduino Uno R3[6] and a similar motor driver, the VNH3SP30[7], result in a global price tag of *EUR 152,26*. Although this does not take into consideration the production cost of the custom parts and assumes the availability of a controlled power source for the motor driver, this value satisfies the requirement for a low-cost device, in the context of medical education equipment.

Concerning joint behavior, the device is capable of varying its mechanical impedance as a

[1] https://www.botnroll.com/pt/sensores/967-weight-sensor-load-cell-0-50kg.html
[2] https://www.botnroll.com/en/flex-pressure-vibration/1638-sparkfun-load-cell-amplifier-hx711.html
[3] https://www.botnroll.com/index.php?id_product=146&controllerp̄roduct&id_lang7̄
[4] https://www.botnroll.com/en/dc-motors-actuators/147-emg49bracket.html
[5] https://www.electrofun.pt/sensores-arduino/modulo-acelerometro-giroscopio-mpu-9250-sparkfun
[6] https://www.ptrobotics.com/arduino/5542-arduino-uno-r3-compatible-ch340-chip-w-usb-cable.html
[7] https://www.tme.eu/pt/details/bb-vnh3sp30/acessorios-para-sistemas-de-arranque/olimex/

function of the force applied to the load cell, its angular position and velocity, and a series of system parameters such as cogwheel position, intensity and directionality, which are defined through code or via serial communications. In this way, the simulator is capable of mimicking some intrinsic features of the wrist that may vary from patient to patient, such as maximum flexion and extension range, as well as features normally verified in patients undergoing DBS such as cogwheel rigidity.

In order to verify the iHandU simulator system outputs, a comparison was performed with the newest iteration of the iHandU wearable device, detailed in [14]. In terms of sensor accuracy, a comparative graph was drawn between the measurements of the iHandU (using the ICM-20948 motion tracking device[8]) and the accelerometer Y-axis readings from our MPU-9250. The experimental setup for this comparison is shown in figure 4.1. The data is then adequately formatted and exported for comparison in MATLAB.

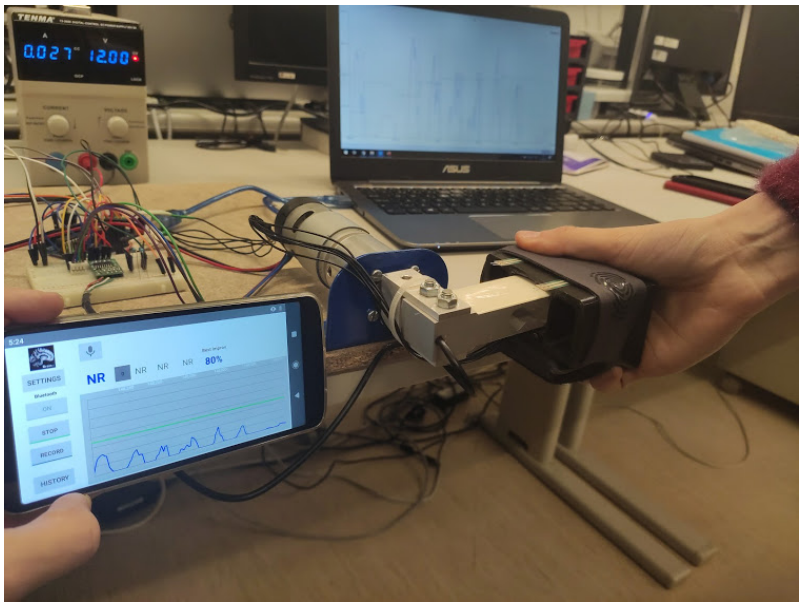

Figure 4.1: Experimental setup for simulator comparison with the iHandU. Simulator data is acquired in the laptop computer via serial port communications. Wearable data is acquired in the mobile device via *Bluetooth*

As the iHandU wearable and iHandU simulator report data asynchronously from one another and at different sampling frequencies (50Hz and 80Hz respectively), relevant signal features in the form of local minimums were temporally matched in figure 4.2 along the duration of ten sets of simulated extensions and flexions, such that $\Delta t \approx 6s$. For this same reason, a full comparison between the signals is difficult, as, say, re-sampling of the simulator signal would still result in an inaccurate representation of the error between values. Instead, a comparison between the relative peaks within each oscillation was performed.

[8] https://www.invensense.com/products/motion-tracking/9-axis/icm-20948/

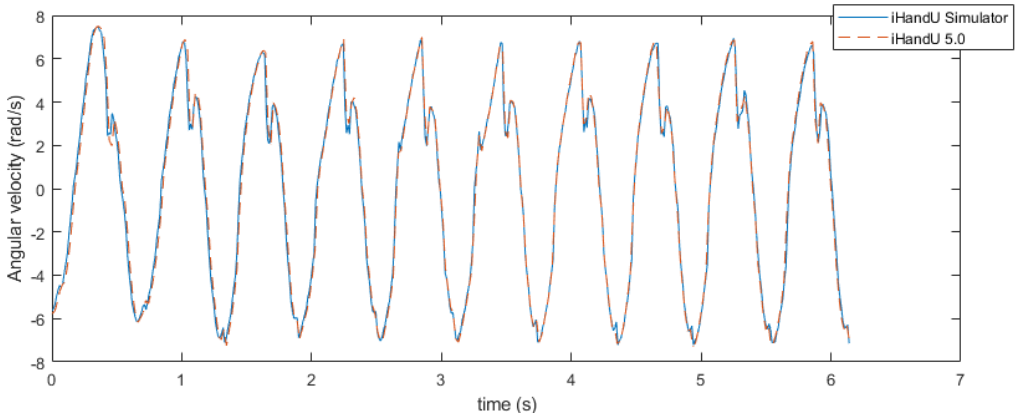

Figure 4.2: Accelerometer signal comparison between the iHandU simulator and the iHandU wearable. The smaller peaks present in each oscillation show the system's reproduction of cogwheel rigidity.

This comparison was achieved by selecting all signal relative peaks with sufficient topographical prominence[9], so as to filter the smaller cogwheel-related peaks, as well as any noise-related peaks. This yielded an average error value of 0.110 rad/s, corresponding to an amplitude error of approximately 1.6% in relation to the mean peak amplitude of the iHandU signal in the same set of samples.

Experimentally, it has been verified that the angular velocity signals measured by the wearable and the simulator are very similar to each other, satisfying our need for comparability.

In its current version, the iHandU wearable is equipped with force sensors, although data acquisition from these sensors is still undergoing implementation. The simulator is already capable of acquiring and reporting force data sensed through the load cell. However, differences between the two sensing methods, such as their differing sensing regions, may invalidate a future force comparison, depending on the exact way the assessment is performed. To ensure future force data comparability once the force sensors are fully implemented in the wearable, the simulator structure was preemptively equipped with the same model of force sensing resistors used in the wearable, *FSR series 400* [14], as shown in figure 4.3.

In order to compare the simulator mechanical output, a similar movement to the one visible on figure 4.2 was performed, and assessments were taken by each of the two most recent iHandU device models to similar results. Concerning fluidity in relation to the motor "off" state, the rigidity scores attributed could reach the maximum value of the improvement percentile scale, which is 80%, however the reliability of this metric is limited as the wearable algorithm is currently insensitive to the user force. Concerning rigidity greater than the motor "off" state, the simulator is capable of providing sufficient torque to ostensibly match any reasonable force that could be applied in the context of a rigidity assessment while drawing a current well within the motor and driver safety values for constant operation ($\leq 3A$).

[9] https://www.mathworks.com/help/signal/ug/prominence.html

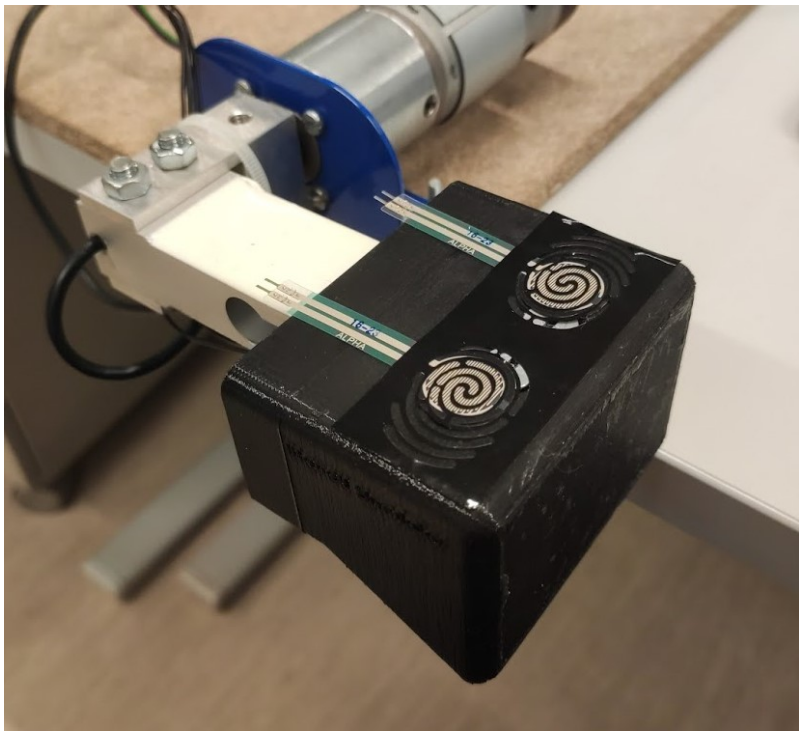

Figure 4.3: Placement of force sensing resistors in the simulator structure.

Chapter 5

Conclusion and Future Work

The rotary simulator for wrist rigidity produced in this work has been shown to present an adequate behavior using the simple gain-based model implemented, according to the currently available wrist kinematic data. In order to provide a full, objective assessment on the validity of its capabilities, records of force data and discussion meetings with clinicians familiar with the assessment are expected to be held in coming months.

In this way, this work has resulted in the creation of a platform for wrist simulation that may now be further explored and utilised by the iHandU development team.

As per the exploratory nature of this work, there is no shortage of possible improvements and hypotheses for future testing. The following are a few, presented as personal suggestions and aimed towards the improvement of this device as a realistic and marketable wrist rigidity simulator.

Creation of a control model. It is expectable that a future iteration of this simulator may be outfitted with a more realistic control model, which can be developed in parallel with future iHandU algorithms, as the implementation of an algorithm using both kinematic and force data is foreseen for the current wearable model [14, 10]. Through use of future data sets, using force data as our sensorial input, and the system kinematic data as our desired simulator output, a system identification approach can be considered [1].

Alternatively, a control model may be developed using data from an existing documented effort to create a viscoelastic mathematical model of the wrist joint in the context of quantification of parkinsonian rigidity. Through use of a device shown in 5.1, this study concludes that the most successful model among those studied for the quantification of parkinsonian rigidity considered one spring constant and one damping constant across all phases [16].

Anatomical realism. The current simulator dimensions are arguably within those of a large human hand, and the hand-like segment consists of a PLA model resembling a fist. Some measures can be taken to improve this aspect of the simulator, such as the use of a synthetic, skin-like coating as seen in section 2.4.2. A review on the average anatomic proportions of a human hand could be

[1] https://www.mathworks.com/help/ident/gs/about-system-identification.html

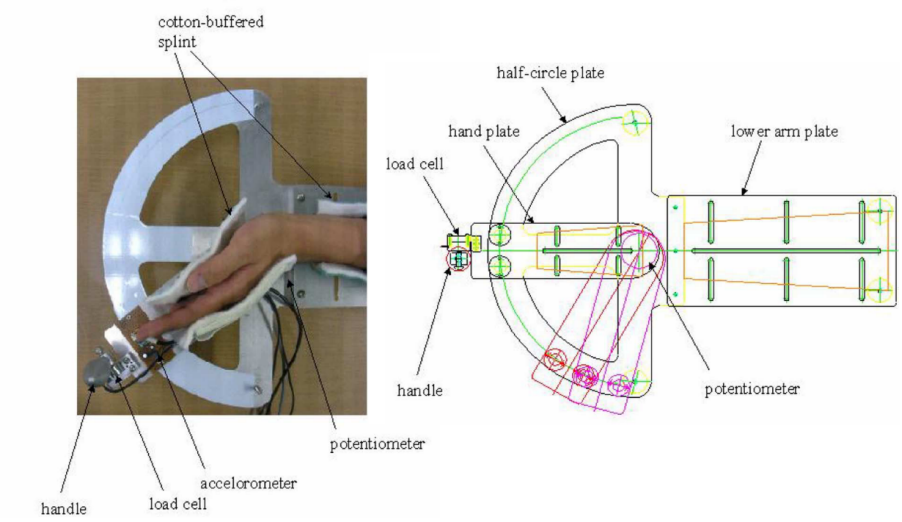

Figure 5.1: Mechanism produced for the creation of a viscoelastic model of the wrist joint by Park et al., extracted from [16]

performed, and not exclusively for aesthetic purposes. The length of the hand-like segment will influence the torque produced as a result of a force applied to the segment extremity, and smaller load cells are available[2]. The attachment of a suitable fixed handlebar to the simulator base in order to serve as a grip in lieu of the patient forearm would prove a simple and welcome addition, as well.

PCB integration. The current version of the simulator displays each component on the simulator base board connected with jumper cables for greater flexibility in the event of any component changes. In the interest of system robustness and marketability, these components may be eventually organized and agglomerated in a Printed Circuit Board (*PCB*) for a more compact form.

Passive and spherical actuation. Passive methods of actuation were considered for application in this simulator, such as the use of brakes or the dynamic braking of an electric motor (section 3.1.2). These could be explored in the future should there be an explicit need for a safer method of actuation that excludes the use of active components. In the context of dynamic braking, the motor non-braking mechanical impedance could be decreased by using a different gear box. In figure 5.2, a modular gear box option[3]is presented.

In conclusion, a mechanical foundation and preliminary control system have been laid out towards a medical education tool for wrist rigidity assessment. Through future development of

[2] https://cdn.sparkfun.com/datasheets/Sensors/ForceFlex/TAL220M4M5Update.pdf
[3] https://www.pololu.com/product/70

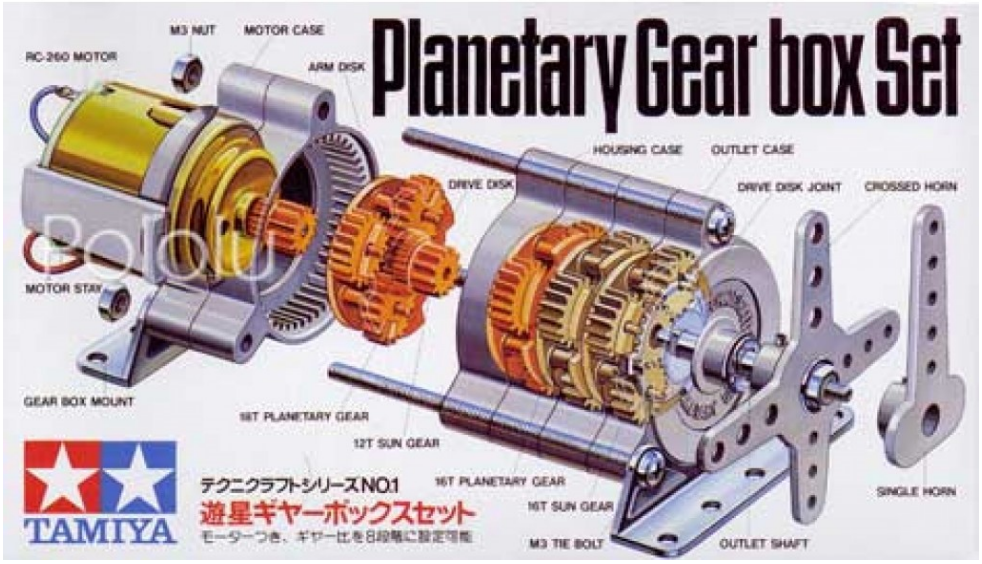

Figure 5.2: Modular planetary gear box by Tamiya Corporation. Source[3]

the simulator resulting from this work, it is hoped that the consistency issue in the training of clinicians may be resolved.

References

[1] Notes from supervisory meetings with Prof. Dr. Paulo Costa, 2019. [Personal Communications].

[2] Deepak Baranwal and T.S. Deshmukh. MR-Fluid Technology and Its Application- A Review. *International Journal of Emerging Technology and Advanced Engineering*, 2(12):563–569, 2012.

[3] Michael P. Caligiuri. Portable device for quantifying parkinsonian wrist rigidity. *Movement Disorders*, 9(1):57–63, 1994.

[4] Pedro Costa, Maria Jose Rosas, Rui Vaz, and Joao Paulo Cunha. Wrist rigidity assessment during Deep Brain Stimulation surgery. In *Proceedings of the Annual International Conference of the IEEE Engineering in Medicine and Biology Society, EMBS*, pages 3423–3426, Milano, Italy, nov 2015. Institute of Electrical and Electronics Engineers Inc.

[5] Houde Dai, Bernward Otten, Jan Hinnerk Mehrkens, and L. T. D'Angelo. A portable system for quantitative assessment of parkinsonian rigidity. In *Proceedings of the Annual International Conference of the IEEE Engineering in Medicine and Biology Society, EMBS*, pages 6591–6594, Osaka, Japan, 2013.

[6] Paolo Ghiglione, Roberto Mutani, and Adriano Chiò. Cogwheel rigidity. *Archives of Neurology*, 62(5):828–830, 2005.

[7] Irving Gottlieb. Practical Electric Motor Handbook. In *Practical Electric Motor Handbook*, pages 1–8, 25, 42–43, 56–57, 115–117. Elsevier, 1997.

[8] David I. Grow, Mengnan Wu, Michael J. Locastro, Sugandha K. Arora, Amy J. Bastian, and Allison M. Okamura. Haptic simulation of elbow joint spasticity. In *Symposium on Haptic Interfaces for Virtual Environment and Teleoperator Systems*, pages 475–476, Reno, Nevada, USA, 2008.

[9] Gael Langevin. InMoov open-source 3D printed life-size robot. *pp. URL: http://inmoov. fr, License: http://creativecommons. org/licenses/by–nc/3.0/legalcode, accessed 20 Jan 2020*.

[10] Elodie Múrias Lopes, Maria do Carmo Vilas-Boas, Duarte Dias, Maria José Rosas, Rui Vaz, and João Paulo Silva Cunha. iHandU: A Novel Quantitative Wrist Rigidity Evaluation Device for Deep Brain Stimulation Surgery. *Sensors (Basel, Switzerland)*, 20(2):s20020331, 2020. Open access publication. DOI:10.3390/s20020331.

[11] Elan D. Louis, Ruth Ottman, and W. Allen Hauser. How common is the most common adult movement disorder? Update on the worldwide prevalence of essential tremor. *Movement Disorders*, 25(5):534–541, 2010.

[12] Tetsuya Mouri, Haruhisa Kawasaki, Yutaka Nishimoto, Takaaki Aoki, Yasuhiko Ishigure, and Makoto Tanahashi. Robot Hand Imitating Disabled Person for Education/Training of Rehabilitation. *Journal of Robotics and Mechatronics*, 20(2):280–288, apr 2008.

[13] Michael S. Okun and Pamela R. Zeilman. *Parkinson's Disease Deep Brain A Practical Guide for Patients and Families*. National Parkinson Foundation, Incorporated, 2014. accessible at https://www.parkinson.org/sites/default/files/attachments/Deep-Brain-Stimulation-Guide-Parkinsons.pdf.

[14] Ana Elisa Oliveira. An innovative wearable device to evaluate motor symptoms during deep brain stimulation surgery. Master's thesis, NOVA University Lisbon, 2019.

[15] Spyridon Papapetropoulos, Heather L. Katzen, Blake K. Scanlon, Alexandra Guevara, Carlos Singer, and Bonnie E. Levin. Objective quantification of neuromotor symptoms in parkinson's disease: Implementation of a portable, computerized measurement tool. *Hindawi*, 2010. Open access publication. DOI: 10.4061/2010/760196.

[16] Byung Kyu Park, Yuri Kwon, Ji Won Kim, Jae Ho Lee, Gwang Moon Eom, Seong Beom Koh, Jae Hoon Jun, and Junghwa Hong. Analysis of viscoelastic properties of wrist joint for quantification of parkinsonian rigidity. *IEEE Transactions on Neural Systems and Rehabilitation Engineering*, 19(2):167–176, 2011.

[17] Susan K. Patrick, Allen A. Denington, Michel J.A. Gauthier, Deborah M. Gillard, and Arthur Prochazka. Quantification of the UPDRS rigidity scale. *IEEE Transactions on Neural Systems and Rehabilitation Engineering*, 9(1):31–41, 2001.

[18] Ludovico Orlando Russo, Giuseppe Airò Farulla, Daniele Pianu, Alice Rita Salgarella, Marco Controzzi, Christian Cipriani, Calogero Maria Oddo, Carlo Geraci, Stefano Rosa, and Marco Indaco. PARLOMA - A novel human-robot interaction system for Deaf-blind remote communication. *International Journal of Advanced Robotic Systems*, 12(5):57, 2015. Open access publication. DOI: 10.5772/60416.

[19] Vicenta Salanova. Deep brain stimulation for epilepsy. *Epilepsy and Behavior*, 88:21–24, 2018.

[20] Bassem Sudki, Michel Lauria, and Flavio Noca. Marine propulsor based on a three-degree-of-freedom actuated spherical joint. In *Third International Symposium on Marine Propulsors*, pages 481–485, Tasmania, Australia, 2013.

[21] Ole-Bjørn Tysnes and Anette Storstein. Epidemiology of Parkinson's disease. *Journal of Neural Transmission*, 124(8):901–905, 2017.

[22] Marie Vidailhet, Marie France Jutras, Emmanuel Roze, and David Grabli. Deep brain stimulation for dystonia. *Handbook of Clinical Neurology*, 116:167–187, 2013.

[23] Noor Ayuni binti Che Zakaria, Takashi Komeda, Cheng Yee Low, and Kaoru Inoue. Emulating upper limb disorder for therapy education. *International Journal of Advanced Robotic Systems*, 11(11):183, 2014. Open access publication. DOI: 10.5772/58893.